Refurbishing the marine parasitoid order Pirsoniales with newly (re)described marine and freshwater free-living predators

Kristina Prokina, Naoji Yubuki, Denis Tikhonenkov, Maria Christina Ciobanu, Purificación López-García, David Moreira

NEW REPRESENTATIVES OF ORDER PIRSONIALES

Refurbishing the marine parasitoid order Pirsoniales with newly (re)described marine and freshwater free-living predators

Kristina I. Prokina[a,b]*, Naoji Yubuki[a,c], Denis V. Tikhonenkov[b,d], Maria Christina Ciobanu[a], Purificación López-García[a] and David Moreira[a]*

a Ecologie Systématique et Evolution, Université Paris-Saclay, CNRS, AgroParisTech, Gif-sur-Yvette, 91190, France
b Papanin Institute for Biology of Inland Waters RAS, Borok, 152742, Russia
c Institut Curie, Université PSL, CNRS UAR2016, Inserm US43, Université Paris-Saclay, Multimodal Imaging Center, 91400 Orsay, France
d University of Tyumen, AquaBioSafe Laboratory, Tyumen 625003, Russia

* Correspondence:
K. I. Prokina, D. Moreira, Ecologie Systématique et Evolution, Université Paris-Saclay, CNRS, AgroParisTech, 12 route 128, Gif-sur-Yvette, 91190, France
e-mail: kristina.prokina@universite-paris-saclay.fr; david.moreira@universite-paris-saclay.fr

ABSTRACT Pirsoniales is a stramenopile order composed of marine parasitoids of diatoms with unique life cycle. Until recently, a single genus, *Pirsonia*, uniting six species, was known. The recent identification of new free-living eukaryotrophic Pirsoniales *P. chemainus*, *Feodosia pseudopoda* and *Koktebelia satura* changed our understanding of this group as exclusively parasitic. However, their cell ultrastructure and feeding preferences were not fully studied due to the death of the cultures. In this study, we re-isolated some of these Pirsoniales and established six new strains exhibiting predatory behavior, including a first freshwater representative. This allowed us to describe five new genera and species, as well as to emend the diagnosis of the order Pirsoniales. 18S rRNA gene phylogenetic analysis revealed the position of new strains within Pirsoniales and their relationships with parasitoid relatives and environmental sequence lineages. Feeding experiments on novel Pirsoniales strains using diverse algal prey showed that they were not able to form trophosomes and auxosomes. The ability of cell aggregation in Pirsoniales was observed for the first time. One of the studied strains contained intracellular gammaproteobacteria distantly related to *Coxiella*. Ultrastructural analyses revealed a more complex cytoskeleton structure in Pirsoniales than previously thought and supported the monophyly of Bigyromonadea and Pseudofungi.

Keywords
Bigyromonadea; eukaryotrophy; 18S rRNA gene phylogeny; protists; Pseudofungi; ultrastructure.

Stramenopiles is a large and highly diverse group of eukaryotes, which includes free-living heterotrophic flagellates, unicellular and multicellular photosynthetic algae (e.g., brown algae, golden algae, xantophytes, diatoms, etc.), and important parasites (oomycetes, *Blastocystis*) (Derelle et al., 2016). They are part of the supergroup SAR (Stramenopiles-Alveolata-Rhizaria) (Adl et al., 2019). However, the phylogenetic relationships of several major stramenopile lineages remain poorly resolved due to the lack of massive sequence data, in particular for heterotrophic representatives, including many MAST (MArine STramenopile) lineages, whose undescribed diversity was predicted by environmental DNA studies (Logares et al., 2012; Massana et al., 2004, 2006, 2009, 2014, 2015).

The biology, morphology, and ecology of many stramenopiles also remain poorly studied. In particular, we know almost nothing about most MAST lineages other than their phylogenetic position in 18S rRNA phylogenetic trees and that they are common in diverse aquatic ecosystems (Logares et al., 2012; Massana et al., 2004, 2006, 2009, 2014, 2015; Simon et al., 2015). It remains to be determined what precise role they play in microbial communities and what the ultrastructural organization of their cells is, although some efforts have been carried out (Cavalier-Smith and Scoble, 2013; Cho et al., 2024; Shiratori et al., 2017). Even long-known groups of heterotrophic stramenopiles, such as Bicosoecida, Labyrinthulea or Hyphochytriomycota, remain poorly studied, and our understanding of entire large taxa is based on scant data from the few described species available, which sometimes leads to incorrect conclusions about the broader ecology and biology of these groups.

An illustrative example is that of the Bigyromonadea, a group of marine heterotrophs comprising a few studied species belonging to the subgroups Pirsoniales and Developea (Cho et al., 2022). Pirsoniales encompasses parasitoid protists initially described in the 1990s and, until recently, included six species in the single genus *Pirsonia*: *P. eucampiae*, *P. diadema*, *P. formosa*, *P. guinardiae*, *P. punctigera*, and *P. verrucosa* (Kühn et al., 1996; Schnepf et al., 1990; Schweikert and Schnepf, 1997). One species, originally described as *Pirsonia mucosa*, was transferred to *Pseudopirsonia* (Cercozoa) according to molecular phylogenetic data (Kühn et al., 2004). Pirsoniales are characterized by a unique life cycle and are adapted to consume large diatom cells. The zoospores are attracted to the diatom hosts by chemical signals and form pseudopodia that penetrate the frustule through one or several frustule openings, e.g., through strutted or labiate processes, openings at the end of the setae, or gaps between girdle bands or less silicified parts of the cingulum (Schweikert, 2015). Subsequently, the pseudopodium forms a special structure inside the host called the trophosome. It digests the host cytoplasm and transports organic matter to the main part of the cell that remains outside – the auxosome. During feeding, auxosomes divide several times, producing secondary auxosomes that attach to each other and to a common trophosome, forming a bouquet-like group of up to 60 descendants (Schweikert and Schnepf, 1997). Several individual zoospores can infect the same diatom cell and their trophosomes can merge. Usually, the Pirsoniales cells retract their flagella during infection, with the exception of *P. eucampiae*, whose flagella are only partially retracted (Kühn et al., 1996). Eventually, after the diatom protoplast is consumed, secondary auxosomes detach and mature into individual zoospores, producing flagella and changing the cell shape from spherical to oval. The trophosomes with residual bodies of undigested chloroplasts remain inside the host (Kühn et al., 1996; Schnepf et al., 1990).

Although ultrastructural data obtained for *P. guinardiae*, *P. diadema*, and *P. punctigerae* confirmed that they belong to stramenopiles, they also emphasized the uniqueness of these organisms (Schnepf and Schweikert, 1997; Schweikert and Schnepf, 1997). Typical stramenopile features included tripartite tubular mastigonemes on the anterior flagellum, tubular mitochondrial cristae, and a helix in the transition zone of the flagella. Unique structures in *Pirsonia* were the presence of cell body hairs and reduced flagellar apparatus (both posterior flagellar roots are fibrous). The kinetosomes are oriented at a right angle to each other and connected by two fibrous bands: one short and wide proximal striated connecting band and one long and narrow electron-dense distal connecting band. The anterior kinetosome is connected to the nucleus by two nuclear bands. Based on these ultrastructural features, Cavalier-Smith created the new order Pirsoniales within stramenopiles, provisionally placing it in the class Bicoecea, phylum Sagenista (Cavalier-Smith, 1998). The ability to form trophosomes and auxosomes was indicated as a main taxonomic characteristic for this order (Cavalier-Smith, 1998). The first 18S rRNA gene phylogenetic analysis confirmed the placement of Pirsoniales in Stramenopiles, but as a sister clade to hyphochytriomycetes, both related to ochrophytes (Kühn et al., 2004). Subsequent 18S rRNA gene phylogenetic analyses

confirmed the closer relationship of Pirsoniales with hyphochytrids, but also with oomycetes and *Developayella elegans* (Cavalier-Smith and Chao, 2006), thus allowing to place them within the phylum Pseudofungi. The authors also placed hyphochytrids, *Pirsonia* and *Developayella* within the class Bigyromonadea.

Further phylogenetic and phylogenomic studies have shown contradictory results regarding Pirsoniales (Aleoshin et al., 2016; Leonard et al., 2018; Noguchi et al., 2016; Thakur et al., 2019; Weiler et al., 2021). The monophyly of Bigyromonadea has not been tested by phylogenomic analysis until recently due to the lack of transcriptomic or genomic data, and Bigyromonadea itself has shown different phylogenetic positions, branching with either Ochrophytes or Oomycetes. Recently, transcriptomic data were obtained from three new pirsoniales, *P. chemainus*, *Feodosia pseudopoda* and *Koktebelia satura*, as well as from four new developean species (Cho et al., 2022). Subsequent phylogenomic analyses confirmed the monophyly of Bigyromonadea, which includes two diverse subgroups, Developea and Pirsoniales. Nevertheless, the position of Bigyromonadea within stramenopiles was not fully resolved. Maximum likelihood multigene trees showed its sister relationship with oomycetes, whereas Bayesian analyses and topology testing were inconclusive (Cho et al., 2022).

In contrast to all previously known Pirsoniales, the new strains studied by Cho et al. (2022) were eukaryovorous predators feeding on bodonid flagellates in culture. However, they did not actively pursue the prey and only partially consumed it (except for one species, *K. satura*), and all the cultures died after a few months of cultivation. Thus, ultrastructural data were not obtained, and the authors did not conduct feeding experiments to determine whether these clones were able to parasitize diatoms and form trophosomes and auxosomes. Nevertheless, Cho et al. (2022) proposed that these Pirsoniales represented motile zoospore stages of parasites capable of facultative eukaryotrophy to survive between host bloom seasons. The morphology of those strains was not studied in detail, and provisional names without formulation of taxonomical diagnoses were provided. These authors also observed some similarities between studied bigyromonadeans and oomycete zoospores in terms of cell morphology, swimming patterns and, especially, the ability to self-aggregate, a feature that was found in developeans for the first time. Taking into account the obtained phylogenomic and morphological results, the authors speculated on the origin of oomycetes, assuming that the ancestor of oomycetes was a phagoheterotrophic amoeboid protist (Cho et al., 2022).

Testing this hypothesis and better understanding the global evolution of stramenopiles will require the characterization of other poorly known lineages. This is all true for Pirsoniales, the diversity, morphology and biology of which have not been sufficiently studied despite the fact that they are one of the major clades of the stramenopile tree. In this study, we reisolated two of the three species studied by Cho et al. (2022) as well as three new pirsoniales from different and geographically distant marine and freshwater habitats. All of them were predatory flagellates that consume diverse prey. 18S rRNA gene phylogeny together with morphological and ultrastructural observations allowed us to describe several new taxa and characterize the morphology and biology of Pirsoniales.

MATERIALS AND METHODS

Strain isolation and culture maintenance

Nine clonal cultures of predatory pirsoniales (Colp-Nor4, Colp-Nor6, Colp-p1, Colp-S9, Kt49-10a, NY0226, Pirs-sm2, Colp-RSA11, and Pirs-vl) were isolated from different marine and freshwater environments (Table 1). Prey cultures were isolated from the same samples or obtained from colleagues (Table 1). Water samples with the upper sediment layer were taken with sterile 15 ml Falcon tubes. The samples were enriched with 1% YT medium (100 mg of yeast extract and 200 mg of tryptone in 100 ml of distilled water as described in the protocol

from the National Institute for Environmental Studies, Japan) to stimulate bacterial growth, and incubated at 15°C. The samples were examined under a light microscope within 10 days in search of predatory flagellated cells. Strains were isolated by picking one cell using a glass micropipette and placed in marine or freshwater media (f/2 diatom media based on filtered and autoclaved marine water (Guillard and Ryther, 1962) and Volvic (France) mineral water, respectively) with cultures of eukaryotic prey at 15°C with a 10h light / 14h dark cycle. All the cultures are currently stored in a collection of live protist cultures in the laboratory Ecologie Systématique Evolution, CNRS, Université Paris-Saclay (except for Colp-RSA11 and Pirs-sm2, which were lost).

For the feeding experiments, diverse eukaryotic prey, including diatom algae, red algae, and heterotrophic flagellates (see Table 2), were used as food sources. Single predator cells were transferred into individual wells of 48-well plates containing 1 ml of enriched prey culture. Experiments with each predator/prey combination were repeated 6 times and observations were carried out for three weeks. If a predator multiplied and no eukaryotic contamination was observed in the prey culture, we assumed the ability of the predator to consume this prey (see Table 2).

18S rRNA PCR amplification, sequence alignment, and phylogenetic analyses

The 18S rRNA genes from all of our strains were amplified using the Platinum Taq polymerase reaction mix (Invitrogen, Thermo Fisher, France) in 25 µl reaction volumes and two combinations of universal eukaryotic primers: A) EK-1F (5'-CTGGTTGATCCTGCCAG-3') and 1520R (5'-CYGCAGGTTCACCTAC-3'); B) EK-82F (5'-GAAACTGCGAATGGCTC-3') and 18S-1498R (5'-CACCTACGGAAACCTTGTTA-3'). PCR amplifications were carried out using a nested approach. For the first PCR, manually isolated single cells (with eight replicates of one cell per reaction for each strain) were added to PCR reaction mix with primer combination A. Then, we used 2 µl of the resulting non-purified PCR products as a template for subsequent PCR reactions using primer combination B. The touchdown amplification steps were as follows: initial denaturing period (95°C for 2 min) followed by 35 cycles of denaturation (95°C for 30 s), annealing (60°C for 30 s in the first cycle, decreasing at 1°C per cycle until reaching 55°C), extension (72°C for 1 min 30 s), and a final extension period (72°C for 5 min). In the case of strain Colp-S9, we needed a third nested PCR reaction (with primers 612F (5'-GCAGTTAAAAAGCTCGTAGT-3') and 1498R) to produce enough amplicon DNA for sequencing. Sanger sequencing of PCR amplicons using forward and reverse primers was performed by Azenta (Leipzig, Germany). For each strain, we used MAFFT (Katoh et al., 2002) with default settings to align forward and reverse sequences and generate a consensus sequence using the cloud-based platform Benchling (https://www.benchling.com/). The resulting 18S rRNA gene sequences were submitted to GenBank under accession numbers PP795565 (strain Colp-Nor4), PP795580 (strain Colp-Nor6), PP795920 (strain KT49-10a), PP795921 (strain Colp-S9), PP795933 (strain NY0226), PP808807 (strain Colp-RSA11), PP808838 (strain Pirs-vl), PP808806 (strain Colp-p1), PP808839 (strain Pirs-sm2), PP795975 (strain str-V), PP795979 (strain diat-RSA1).

The obtained 18S rRNA gene sequences were added to a dataset containing 97 sequences (collected from the GenBank database) representing main stramenopile clades, as well as seven outgroup sequences (alveolates and rhizarians). We also constructed a reduced dataset containing 75 sequences representing all Gyrista clades with and without environmental sequences. Multiple sequence alignments were constructed using the L-INS-i algorithm in MAFFT v.7.475 (Katoh and Standley, 2013). Alignments were trimmed using trimAl v.1.2 (Capella-Gutiérrez et al., 2009) with the gappyout method. The numbers of analyzed sites after trimming were 1,437 bp for the full dataset, 1,514 bp for the reduced dataset, and 1,504 bp for the dataset with environmental sequences.

To infer Bayesian phylogenetic trees, the parallel MPI version of MrBayes v.3.2.7a (Ronquist et al., 2012) was used with four categories of gamma-distributed among-site rate variation under the GTR+I+GAMMA4 substitution model. To calculate posterior probabilities of individual nodes, four independent Metropolis-coupled Markov chains were run for 20 million generations and summarized after the 50% burn-in. The convergence of log-likelihood values and model parameters for chains was verified using a plot and convergence diagnostics provided by the MrBayes sump utility. Maximum likelihood phylogenetic trees were inferred using IQ-TREE v.2.2.2.6 (Nguyen et al., 2015) with 1,000 nonparametric bootstrap pseudoreplicates under the GTR+GAMMA+I substitution model. Trees were visualized using the cloud-based platform iTOL (https://itol.embl.de/).

Microscopy

Light microscopy observations were made using an inverted Zeiss Axiovert 40 CFL microscope equipped with phase contrast objectives (20× and 40×) and an upright Zeiss Axioplan 2 microscope equipped with an oil-immersion DIC objective (100×) and a water-immersion phase contrast/DIC N-Achroplan objective (63×). Videos were recorded with a Sony α9 digital camera. Images as still frames were captured using a Light Alloy video player (https://light-alloy.com/).

For epifluorescent microscopy observations, live cells of *Feodosia pseudopoda* strain NY0226 were incubated in the dark for 1 h with Hoechst 33342 (Molecular Probes, Thermo Fisher, France) at a final concentration of 10 µg/ml. The cells were imaged directly in the staining solution without washing with a Zeiss Axioplan 2 epifluorescence microscope equipped with a 49 mm filter set.

For scanning electron microscopy (SEM), 1 ml aliquots of cell-rich cultures were mixed with 1 ml of 4% glutaraldehyde (final concentration of 2%) diluted in sterile sea water (for marine strains) or 0.2 M sodium cacodylate buffer, pH 7.2 (for the freshwater strain Pirs-vl). After that, the mixture was deposited on a 9-mm circular cover slip coated with poly-L-lysine and fixed for 30 min. After fixation, the cells were washed with 0.2 M sodium cacodylate buffer (pH 7.2) and dehydrated in a graded series of ethanol baths (30%, 50%, 70%, 80%, 90%, 100% ×3 times, 10 min each). Then, the coverslips with cells were washed with 100% hexamethyldisiloxane three times for 15 min and subsequently dried at room temperature. Dry coverslips were mounted on aluminium stubs, coated with platinum, and observed using a GeminiSEM 500 (Carl Zeiss, Germany) scanning electron microscope.

For investigation of the cell ultrastructure in transmission electron microscopy (TEM), aliquots of cell-rich cultures were mixed with glutaraldehyde (sample-to-fixative ratio 1:1) diluted in cacodylate buffer (1.25-2% final concentration) and fixed for 2 h on ice or at room temperature. After fixation, the cell pellets were collected by centrifugation for 10 min at 5,000 *g*, washed with 0.2 M cacodylate buffer and fixed with 2% osmium tetroxide in 0.2 M cacodylate buffer for 1 h at room temperature. Alternatively, a mixture of both fixatives, glutaraldehyde (2.5% final concentration) and osmium tetroxide (1% final concentration), in 0.2 M cacodylate buffer was added to the cell cultures and incubated for 30 min on ice. After dehydration in an alcohol series (30, 50, 70, 80, 90, 96, 100% ×2 times, 10 min each) and acetone (100% ×2 times, 10 min), the pellets were embedded in Low Viscosity resin (EM 0300 Sigma-Aldrich). Ultrathin sections (70 nm) were prepared with a Leica EM UC6 ultramicrotome (Leica Microsystems, Germany) and observed using a JEM 1400 transmission electron microscope (JEOL, Japan).

16S rRNA gene PCR amplification and phylogenetic analysis of the bacterial endosymbiont of strain NY0226

The 16S rRNA gene of endosymbiotic bacteria was amplified with Platinum Taq polymerase reaction mix (Invitrogen, Thermo Fisher, France) in 25 µl reaction volumes and two combinations of universal bacterial primers: A) 27F (5'- AGAGTTTGATCCTGGCTCAG-3') and 1492R (5'- TACCTTGTTACGACTT-3'); B) 63F (5'- CAGGCCTAACACATGCAAGTC-3') and B-1492R. PCR amplifications were carried out using a nested approach. For the first PCR, we added manually isolated and three times washed single cells of strain NY0226 (eight replicates) to a PCR reaction mixture containing primer combination A. Then, we used 1 µl of a 50-fold dilution of the resulting non-purified PCR products as a template for subsequent PCRs using primer combination B. The touchdown amplification steps were as follows: initial denaturing period (95°C for 2 min) followed by 35 cycles of denaturation (95°C for 30 s), annealing (60°C for 30 s in the first cycle, decreasing at 1°C per cycle until reaching 55°C), extension (72°C for 1 min 30 s), and a final extension period (72°C for 5 min). Sanger sequencing of eight amplification products was performed by Azenta (Leipzig, Germany). We used MAFFT (Katoh et al., 2002) with default settings to align the sequences and obtain a consensus sequence using the cloud-based platform Benchling (https://www.benchling.com/). The resulting 16S rRNA gene sequence was submitted to GenBank under accession number PP809757.

The new 16S rRNA gene sequence was added to a dataset containing 101 gammaproteobacterial sequences and seven sequences from Alphaproteobacteria as an outgroup and aligned using MAFFT with default settings (Katoh et al., 2019). Ambiguously aligned positions were trimmed off with trimAL v.1.2 (Capella-Gutiérrez et al., 2009) using a gap threshold of 40% and a minimum percentage of the positions in the original alignment to conserve of 20%. The number of analysed sites after trimming was 1,506 bp. Maximum likelihood phylogenetic trees were inferred using IQ-TREE v.2.2.2.6 (Nguyen et al., 2015) with 1,000 nonparametric bootstrap pseudoreplicates under the best fit model (TPM3+R6 model) determined by the in-built ModelFinder (Posada and Crandall, 1998). The tree was visualized using the cloud-based platform iTOL (https://itol.embl.de/).

RESULTS

18S rRNA gene phylogenetic analysis of new Pirsoniales strains

Using single-cell PCR, we amplified and Sanger-sequenced 18S rRNA genes from nine Pirsoniales strains. The lengths of amplicon sequences were as follow: 1,611 bp (KT49-10a), 1,664 bp (NY0226), 1,055 bp (Colp-S9), 1,644 bp (Colp-p1), 1,567 bp (Pirs-sm2), 1,593 bp (Pirs-vl), 1,641 bp (Colp-RSA11), 1,629 bp (Colp-Nor6), and 1,642 bp (Colp-Nor4).

Preliminary BLAST (Altschul et al., 1990) searches against the nonredundant (nr) GenBank database indicated that the new Pirsoniales were similar to *Pirsonia* spp., sharing 94.71-99.94% identity in the 18S rRNA sequences (Table S1). Therefore, we prepared a multiple sequence alignment containing the newly obtained nine sequences and representative sequences of Pirsoniales and Gyrista (Stramenopiles) for Maximum likelihood (ML) and Bayesian (BI) phylogenetic analyses (Figure 1, S1, S2). Both analyses placed our strains within Pirsoniales with full statistical support. The three studied strains (NY0226, Colp-S9, and KT49-10a) grouped with *Feodosia pseudopoda* strain Chromo-2 with full support (Figures 1, S1, S2) and shared 98.86-99.91% 18S rRNA nucleotide identity with this species (Table S1), suggesting that they likely belong to the same species. A marine strain, Colp-p1, formed a sister lineage to the *Feodosia* clade, separated from the known genera of Pirsoniales. It therefore represented a new genus and species that we named *Bordeauxia parva* gen. et sp. nov. The 18S rRNA gene sequences of two freshwater strains, Colp-RSA11 and Pirs-vl, were almost

identical (99.94% nucleotide identity) and formed an independent clade from other genera, sister to the *Feodosia* and *Bordeauxia* grouping. We propose that these strains represented a new genus and species, *Bullionia fluviatilis* gen. et sp. nov. Two of the studied strains (Colp-Nor4 and Colp-Nor6) grouped with the species *Koktebelia satura* strain Chromo-2 and shared 98.98-99.66% 18S rRNA nucleotide identity with it (Table S1). Finally, the marine strain Pirs-sm2 formed a sister lineage to the clade uniting the representatives of the parasitoid family Pirsoniaceae, thus representing a new genus and species, *Noirmoutieria diatomophaga* gen. et sp. nov. The phylogenetic analyses that included environmental sequences (Figure S1) illustrated some undescribed diversity in the order Pirsoniales in natural environments, closely related to the genera *Noirmoutieria*, *Koktebelia* and *Bullionia*.

Overall morphology and feeding behavior

All studied strains exhibited a common morphological plan but possessed some characteristic differences from each other and from previously described Pirsoniales (Figures 2-4, Table S2). All strains were free-living colorless flagellates with elongated oval non-flattened cells but could undergo significant changes in cell shape depending on the shape of the swallowed prey (Video S1). The starved cells tended to be small (Figures 3B,R, 4D). All the strains had a longitudinal groove on the ventral side of the cell (Figures 2B, 3E,N,P,V, 4B). Two flagella were inserted subapically or almost laterally from a ventral bulge (protrusion) located in the middle region of the ventral groove and were directed oppositely (Figures 2B, 3A,B,G,H,N,R,U, 4C-E), the anterior flagellum (AF) directed anteriorly and the posterior flagellum (PF) directed posteriorly. In this way, the anterior part of the ventral groove looked like the subapical anterior notch. Well-fed cells usually possessed large food vacuoles in their posterior part (Figures 3A,H,S, 4C,D) and their cytoplasm was filled with round refractive granules of reserve material, such as lipid droplets, which were also observed in thin sections (see below). Characteristic cell movements were a distinctive feature for all Pirsoniales. Cells swam in a straight line without rotation, with jerking movements and sudden sharp changes in direction, or attached to a substrate with the posterior flagellum while the anterior flagellum beat quickly (Video S1). Flattened and non-flattened resting cells varied in shape (Figures 3F,L,M,O-T,V,Y-AB, 4B) and their flagella usually made slow sinusoidal movements. Swimming cells could be found in the water column; however, they were mostly concentrated at the bottom of the Petri dishes used for observations.

Unlike the previously described parasitoid *Pirsonia*, the new strains were able to swallow eukaryotic prey entirely (with some exceptions for the strain Colp-S9, see below) using a posterior pseudopodium. Our feeding experiments showed that the new strains consumed a wide range of eukaryotic prey (Table 2) depending on the strain, from a single acceptable prey to almost any proposed prey, and with varying growth success depending on the suitability of the proposed prey.

***Bordeauxia parva* strain Colp-p1 (Figures 2A,B, 3A-F)**

Cells with a weakly pronounced longitudinal ventral groove (Figure 3E), but noticeable ventral bulge and anterior notch (Figure 3A,B). Cells are 6.5-14.0 μm in length and 4-8 μm in width. The starved cells are more elongated with a narrowed posterior end (Figure 3B). The AF is 2-2.5 times longer than the cell, and the PF is 1-2 times longer than the cell. The AF is acronematic, and both flagella are covered with hairs (Figures 2A). The food vacuoles and refractive granules of reserve material are positioned in the posterior part of the cell (Figure 3A-C). Small pointed posterior pseudopodia are seen on some of the attached cells (Figure 3C,D). Resting cells are oval, with slowly waving flagella directed sideways or backwards (Figure 3E,F). From the prey offered here, *Bordeauxia parva* feeds exclusively on the colorless chrysophyte alga *Paraphysomonas lucasi* Scoble et Cavalier-Smith, 2014 strain str-V (Table 2). The cell population can reach high numbers in culture with abundant prey.

***Bullionia fluviatilis* strains Pirs-vl and Colp-RSA11 (Figures 2C-E, 3G-M)**

Cells are oval but may take the shape of the diatom prey they swallow (Figure 3I-K, Video S1). Starved cells with narrowed anterior and posterior ends (Figure 3G). Cells are 8-15 μm in length (up to 25 μm when a large diatom cell is consumed) and 6.5-12 μm in width. The single contractile vacuole is located close to the anterior end of the cell (Figure 3G-M). The ventral groove is poorly developed, and the ventral bulge is well pronounced (Figure 3G,H). AF is 1-1.5 times longer than the cell, and PF is very long, up to 4 times longer than the cell body (20-55 μm in length). The AF bears a short acroneme (Figure 2C,E). Well-fed cells contain many large round refractive granules of reserve material; some cells are fully filled with them (Figure 3L,M). Resting cells (Figure 3L,M) are usually oval, rarely round and flattened (Figure 3L). The flagella of resting cells are coiled near the cell body and remain motionless or very slowly wriggle in sinusoids.

Strain Colp-RSA11 feeds on the heterotrophic flagellate *Bodo saltans* Ehrenberg, 1832, but the culture died soon after isolation. Numerous attempts to re-isolate this strain from the same sample on diverse eukaryotic prey, including the green alga *Pseudomuriella engadinensis* (Kol et Chodat, 1934) Fuciková et al., 2011, the xanthophyte alga *Tribonema gayanum* Pascher, 1925, the naked amoeba *Paravanella minima* Kudryavtsev, 2014, and the chrysophyte heterotrophic flagellate *Spumella* sp., were unsuccessful. The strain Pirs-vl (Table 1) was isolated from another sample and fed on the freshwater diatom *Stephanocyclus meneghiniana* (Kützing, 1844) Kulikovskiy et al., 2022 (strain diat-RSA1) as a prey.

***Koktebelia satura* strains Colp-Nor4 and Colp-Nor6 (Figure 3N-T)**

Cells are 10.5-16 μm in length and 8-13 μm in width. The AF is 1.5 times longer than the cell, and the PF is 1.5-2.5 times longer than the cell. Starved cells with a noticeable anterior notch and a ventral bulge from which flagella emerge (Figure 3R). Resting cells usually maintain an oval shape and possess a visible longitudinal ventral groove (Figure 3O,P, Video S2). Sometimes they produce several finger-like pseudopodia (Figure 3Q, Video S2). Flagella of the resting cells can extend into longitudinal planes and quickly undulate so that the flagella appear to double (Figure 3O, Video S2), or they can be pulled to the cell body and slowly wriggle sinusoidally (Figure 3R). Cells form clusters of resting cells on the substrate in starving cultures (Figure 3T, Videos S3). Despite 1% nucleotide dissimilarity in 18S rRNA gene sequence, both strains did not show any differences in morphology or pattern of cell movement and had identical food preferences (Table 2).

The strains consumed almost any prey offered to them, including all heterotrophic flagellates, almost all red algae (except for one species, *Galdieria* sp., which was partially consumed but predators reproduce slowly, and the culture eventually died), and most diatoms of small size suitable for swallowing.

***Noimoutieria diatomophaga* strain Pirs-sm2 (Figure 3U-AB)**

Cells are elongated with a narrowed anterior end (Figure 3U,Y) and a well-pronounced longitudinal ventral groove (Figure 3V, Video S4). Cells can change shape after swallowing diatom prey (Figure 3W). Cells are 9-13 μm in length and 6-10 μm in width. AF is 2-2.5 times longer than the cell, and PF is 2.5-3.5 times longer than the cell. Cells rarely shed off flagella (Figure 3V, Video S4). Resting cells are oval, round and irregular in shape (Figure 3V,Y-AB), sometimes without flagella (Figure 3AB). Strain Pirs-sm2 consumed several species of diatoms and bodonids (Table 2) and reproduced slowly, never reached a high density in culture, and eventually died after a year of cultivation.

***Feodosia pseudopoda* strains Colp-S9, KT49-10a, and NY0226 (Figures 2F-H, 4)**

Cells with well-developed longitudinal ventral groove (Figure 4B, Video S5), 12-22 μm in length and 9-16 μm in width. Cells can change shape greatly after swallowing diatom prey (Figures 4E,F,G-J). Rarely produce finger-like pseudopodia at any part of the cell body (Figure 4A). Resting cells are oval, round or irregular. Both flagella are 1.5-2 times longer than

the cell (Figure 2F,G). Well-fed cells (Figure 4C) can be significantly larger than starved cells (Figure 4D).

Feodosia pseudopoda consumes a variety of prey such as diatoms, red algae and bodonids (Table 2). The grow success of the studied strains vary depending on the prey; they grow best on the diatom *Attheya* sp. and *Chaetoceros neogracile*. In general, the prey range for strain NY0226 slightly differs from other *Feodosia* strains (Table 2). When feeding on small diatoms such as *Attheya* sp., the diatom frustules are compressed into compact lumps inside the predator cell, sometimes accumulated from several prey cells, and subsequently excreted. Such lumps can be found on the bottom of the culture Petri dish (Figure 4L,M).

Cells of the Colp-S9 strain are able to consume large diatoms (up to 100 µm in length), such as *Licmophora* sp., *Coscinodiscus radiatus* and cf. *Pinnularia* sp. (Figure 4G-J,N-S) using two different strategies. In the case of *Licmophora* sp. (Figure 4G-J), the predators are able to engulf almost the whole diatom, which may reach up to 45 µm in length. This feeding strategy was very successful, and all the diatoms in the culture were consumed. After feeding, the unchanged empty frustules were released by the predator (Figure 4K), in contrast with the deformed frustules of *Attheya* sp.

In the case of *Coscinodiscus radiatus* (Figure 4N-Q) and cf. *Pinnularia* sp. (Figure 4R,S), the diatoms were too large to be swallowed, and the predators used another strategy. They attached to diatoms and penetrated with broad pseudopodia through some of the wide openings of the diatom frustules. It is unclear which openings were used to reach the diatom protoplast; however, openings should be large enough to allow parts of the protoplast and individual chloroplasts to be transported outside the diatom frustule, as visible in diatom cells after predator attack (Figure 4T). As confirmation of this, we observed large food vacuoles with chloroplasts in the attached predator cells outside the diatom frustules (Figure 4O-Q), but we never observed the formation of trophosomes. We hypothesize that *Feodosia* uses thin or less silicified parts of the diatom cingulum for penetration, possibly during the diatom division process when the cingulum becomes vulnerable. Several individual cells can attack one diatom. Not all diatom cells are attacked in culture, and some diatom cells seem to be more suitable for *Feodosia* than others. Flagella of the predator always remain full length and actively beating.

The strains Colp-S9 and KT49-10a can form giant irregularly shaped multinucleated cells with several sets of flagella in the presence of a large amount of diatom prey (Figure 4V-X, Videos S6, S7). These unusual forms are the result of several consecutive incomplete cell divisions when daughter cells remain connected to each other by posterior ends or by long thin pseudopodia. Often, such cells can share a common large food vacuole (Figure 4V-X, Video S7) that is much larger than a single prey cell and represents a lump of accumulated deformed diatom shells and undigested protoplasts. With a decrease in the number of prey cells, the formation of multinucleated cells gradually fades and disappears.

We also observed self-aggregation of cells in strain KT49-10a (Figure 4U, Video S8) when cells reached large numbers. Individual cells were actively attracted and merged into a single mass as opposed to the above-described incomplete division.

Ultrastructure of *Bordeauxia, Feodosia and Bullionia*

***Bordeauxia parva* (Figure 5, 6, 7)**

Cells are covered with hair-like structures of about 0.2 µm in length (Figures 5A,C,F). The nucleus is elongated or pear-shaped (Figure 5A), 2.5-3.5 µm long and 1.5-2 µm wide. Its narrowed part bears two papillae (Figure 6B) connected with the posterior kinetosome by fibrous bands (see below). Single nucleolus situated asymmetrically in the widest part of the nucleus. Numerous elongated mitochondria are evenly distributed in the cell and contain tubular cristae (Figures 5A,D,E) with a central filament in every crista (Figure 5E, insert). Large flattened vesicles underlying the plasmalemma (Figure 5A-C, 6R) tend to swell during

fixation, as the nucleus envelope and endoplasmic reticulum (ER). Some flattened vesicles contain flocculent material (Figure 5C) that may represent a fixation artifact. The cytoplasm contains many lipid droplets 0.3-0.5 μm in diameter (Figure 5A,B,E) and microbodies (Figure 5I) possibly involved in lipid biosynthesis. The Golgi apparatus, with numerous small vesicular bodies (Figures 5G, 6R), is located anterio-ventrally in close connection with the nucleus and kinetosomes.

The AF is covered with tubular mastigonemes, sometimes visible on thin sections (not shown). The PF is covered with simple short hairs similar to the hair-like structures covering the cell surface (Figure 5F). The flagella are frequently shed off during fixation. Tubular mastigonemes are found in dilations of endoplasmic reticulum (Figure 5A,H).

Flagellar kinetosomes have cartwheel structures in the proximal part (Figure 6B). The transition zone of the kinetosomes contains a transverse plate inside axoneme and a prominent annular connection outside the axoneme, both at the same level (Figure 6A). The axosome is located just above the transverse plate, sometimes with a central electron-dense plate (Figure 6A). A large and prominent central dense hub is located below the transverse plate (Figure 6A). An indistinct single transitional helix with about 3-5 gyres is placed above the transverse plate inside the doublets (Figure 6A). The distal part of the kinetosome is surrounded by transitional fibers visible on both longitudinal (Figure 6A) and transverse sections (Figure 6E).

A schematic illustration of the flagellar apparatus is shown in Figure 7. The kinetosomes diverge to each other in wide angle, of about 120° (Figure 6C,F-N, 7). The proximal part of the posterior kinetosome (k1) is shifted to the side of the anterior kinetosome (k2) (Figures 6F-N, 7). The kinetosomes are not it the same plane and k2 is slightly turned to the left. The kinetosomes are connected to each other by two fibrous bands. A short and wide proximal striated connecting band is adjacent to the proximal ends of kinetosomes (Figures 6L,N, 7) and a long and narrow distal connecting band is located closer to the plasmalemma and connects the distal parts of the kinetosomes (Figures 6C, 7). Each kinetosome is supported by some additional osmiophilic materials. K1 is connected to the nucleus by two nuclear bands that run from both sides from the proximal part of the kinetosome to the nuclear papilla (Figure 6B). Several microtubules are originated in this region and directed to the narrow part of the nucleus (Figure 5J-L).

There are four microtubular roots associated with the kinetosomes. Two microtubular roots are associated with k1, corresponding to r1 and r2 in stramenopiles (Moestrup, 2000; Yubuki and Leander, 2013). They originate from the left and right sides of k1 and are connected proximally with each other by the same fiber, which passes near the kinetosome junction closer to k1 (Figures 6B,E,K, 7). Both r1 and r2 are directed posteriorly along the left and right edges of the ventral groove, respectively (Figures 6J-N). The left posterior root (r1) originates from the left side of k1 (Figures 6D-N, 7) and consists of 3-5 microtubules. The right posterior root (r2) originates from the right side of k1. It consists of 8-9 microtubules oriented in semicircle in its proximal part (Figures 6B,D, 7) and of fibrous core material inside the semicircle, which originates from k1 (Figure 7). The fibrous core material terminates in the middle part of r2, while the r2 microtubules separate into two flattened parallel rows (Figure 7). Both posterior roots meet with each other as soon as the ventral groove terminates and become parallel (Figure 6O).

Two anterior microtubular roots are associated with k2. A large and prominent right anterior root (r3) originates near the right proximal end of k2 and is directed clockwise to the anterior pole of the cell along the anterior part of the ventral groove (Figures 6J,P,Q, 7). It consists of three microtubules, reinforced with fibrous material, and several secondary microtubules (ribs) extending perpendicular to the three main microtubules towards the right-dorsal side of the cell (Figures 6J,K,P,Q, 7). An inconspicuous right anterior root r4 consists

of 1-2 microtubules (Figure 7). It originates from the left side of k2 and is directed to the left under the plasmalemma, perpendicular to r3 (Figures 6R, 7).

***Feodosia pseudopoda* strains NY0226 (Figure 8A-H) and KT49-10A (Figure 8I-P)**

As in *Bordeauxia parva*, cells are covered with hair-like structures of about 0.2-0.25 μm in length (Figure 8B). Tubular mastigonemes are visible in dilated parts of the ER (Figure 8E,I). The round nucleus is 2.5-3 μm in diameter (Figure 8A,I) with a slightly asymmetrical nucleolus. Two small nuclear papillae (protrusions) are located near the kinetosomes (Figure 8G,H,K) and associated with two nuclear bands (see below). Sometimes large multinucleated cells are found on thin sections (not shown). Numerous elongated mitochondria with tubular cristae, each containing a central filament, were evenly distributed throughout the cell (Figure 8L). In contrast with *B. parva*, this species does not contain flattened cortical vesicles. Cells of strain NY0226 contained numerous endosymbiotic bacteria located in the cytoplasm (more than 70 bacteria in each host cell). The size of these bacterial cells is about 0.7-1×0.25 μm (Figure 8A,D,E). NY0226 cells also contain large spherical vesicles with flocculent material (Figure 8A,C), mostly on periphery of the cells, and flattened vesicles with similar flocculent material around the nucleus (not shown). Cells of strain KT49-10a are filled with numerous small vesicles (Figure 8I,J). Both strains have microbodies (Figure 8A,C), multivesicular bodies (Figure 8B), and lipid droplets of 0.7-2 μm in diameter (Figure 8J). Food vacuoles contain undigested crumpled diatom frustules (Figure 8J).

Although we did not study the flagellar apparatus of *F. pseudopoda* in detail, we found many similarities in its structure with *B. parva*. Kinetosomes are located in different planes and diverge in a wide angle of about 120° (Figure 8K,M). The proximal end of k1 is shifted to the side of k2 (Figure 8N-P). The transition zone contains a transverse plate with a sometimes visible electron-dense central thickening (Figure 8M). The prominent annular connection is slightly displaced distally to the transverse plate (Figure 8K,M-P). A single transitional helix with 3-5 gyres is located inside the axoneme above the transverse plate (Figure 8K,M-P). The axosome and central dense hub are adjacent to the transverse plate from distal and proximal sides, respectively (Figure 8K,M). Probable acorn-V filaments are sometimes visible at the level of the proximal end of the central dense hub (Figure 8K). The proximal part of the kinetosome has cartwheel structure (Figure 8K,M). Transitional fibers are visible outside the distal part of the kinetosomes, below the annular connection (Figure 8K). The kinetosomes are connected to each other by a proximal striated connecting band (Figure 8K) and a distal connecting band (Figure 8M). The k1 is connected to the nucleus by two long and thin nuclear bands (Figure 8G,H).

The posterior microtubular roots have similar structure with those in *B. parva*. Roots r1 and r2 are connected proximally by fibrous material with k1 (Figure 8N) and both are directed backwards along the left and right edges of the ventral groove (Figure 8N-P). The right posterior root (r2) consists of about eight microtubules oriented in semicircle in its proximal part (Figure 8F) and a core fibrous material inside this semicircle (Figure 8F,N-P).

***Bullionia fluviatilis* strain Pirs-vl (Figure 9)**

Cells are covered with hair-like structures about 0.2 μm long (Figure 9F,H-J). The nucleus is roundish or irregular (Figure 9A,B), 2.5-3.5 μm in diameter and with a slightly asymmetric nucleolus. Two prominent nuclear papillae (Figure 9A,G-I) connect the nucleus with k1 by long and striated nuclear bands (Figure 9D,G-I). Elongated mitochondria contain a dense matrix and tubular cristae with central filaments (Figure 9A-C). The Golgi apparatus, with numerous vesicular bodies (Figures 9D,H-J), is located anterior-ventrally, in close connection with the nucleus and flagellar kinetosomes. Large lipid droplets (up to 2 μm) are found in the posterior part of the cell (Figure 9A).

Kinetosomes are oriented in a wide angle in different planes (Figure 9D,E). Their transition zones consist of a transverse plate (Figure 9D,E) with associated electron-dense

central thick region visible on some sections (Figure 9E). A dense annular connection is located almost at the same level as the transverse plate outside of axoneme (Figure 9D,E). A single transitional helix with six gyres (Figure 9D,E) is located inside the axoneme above the transverse plate. The axosome and central dense hub are adjacent to the transverse plate from distal and proximal sides, respectively (Figure 9D,E). A probable acorn-V system is visible at the level of the proximal end of the central dense hub, right after the triplet microtubules are replaced by doublets (Figure 8K). The proximal part of the kinetosome has cartwheel structure (Figure 9B). The kinetosomes are connected to each other by a proximal striated connecting band (not shown) and a distal connecting band (Figure 9D). Posterior microtubular roots are connected by additional fibers (Figure 9H-J). The left posterior root r1 consist of about 4 microtubules arranged in a flat row (Figure 9F,H-J). The right posterior root r2 consists of about 8-9 microtubules oriented in semicircle in its proximal part and a core fibrous material inside the semicircle (Figure 9F,H-J).

Bacterial endosymbiont of *Feodosia pseudopoda*

Using single cell picking and PCR, we isolated eight cells of strain NY0226 and amplified and Sanger-sequenced the 16S rRNA gene of the intracellular bacterium observed in this species (see above). The amplicon sequence was 1,388 bp long. Preliminary BLAST (Altschul et al., 1990) searches against the nonredundant (nr) GenBank database retrieved the obligate intracellular bacterial pathogen *Coxiella burnetii* as the first hit. Therefore, we included this sequence in a multiple sequence alignment containing representatives of the main Gammaproteobacteria lineages and reconstructed a ML phylogenetic tree. Phylogenetic analysis placed the endosymbiont within a fully supported clade of marine environmental sequences which was sister, albeit with moderate support, to *Coxiella* species (Figure 10A).

Using Hoechst fluorescent DNA staining, we visualized the bacterial endosymbionts inside the four-nucleated host cells under a fluorescence microscope (Figure 10B-D). The number and size of the intracellular bacteria matched the results obtained from the TEM thin sections (Figure 8A,D,E).

DISCUSSION

Feeding behavior of predatory and parasitoid Pirsoniales

Pirsoniales is a group of marine parasitoids of diatoms with unusual life cycle adapted to consume large diatom cells covered in hard siliceous frustules. A unique morphological characteristic of this group is the separation of the cell into the main part (the auxosome), which remains outside the host frustule, and the trophosome, whose function is only to digest diatom protoplasts and transport disintegrated food to the auxosome through a very thin thread.

Pirsonia species have traditionally been considered parasitoids because they depend on their host to complete their life cycle and the host almost always dies after an attack (Anderson and May, 1978; Kühn et al., 1996; Schweikert, 2015; Skovgaard, 2014). The first observation of predation (i.e., swallowing and digesting the whole prey cell) in the order Pirsoniales was poorly documented (Cho et al., 2022). However, now we can assert with confidence that predation of small diatoms and other protists is not only as common as parasitism in the order Pirsoniales, but even prevails (given the larger number of identified predatory genera). The assumption about the facultative nature of predation in the previously studied *Feodosia pseudopoda* and *Koktebelia satura* (Cho et al., 2022) seems unlikely. These species survive well on a variety of prey, and the success of reproduction and food consumption vary greatly depending on the prey (Table 2). It is not surprising that previously studied predatory Pirsoniales did not actively pursue the bodonid prey *Procryptobia sorokini*, as also observed in our feeding experiments (one strain, NY0226, did not consume this prey at all). On the basis

of our observations, it seems that algal prey is preferred by these species. All our cultures, except for *Noirmoutieria diatomophaga*, were maintained for several years, which indicates that they are stable and that their prey are suitable for prolonged growth. Facultative predation still needs to be examined for *Pirsonia chemainus* and *Noirmoutieria diatomophaga* because neither species survived in culture, and feeding experiments have been carried out partially for *Noirmoutieria diatomophaga* (without experiments on large diatoms) or are completely absent for *Pirsonia chemainus*. However, it is interesting to note that the parasitoid *Pirsonia* is closely related to organisms capable of effective predation, which allows us to assume that parasitism has only recently evolved in this group.

To further confirm that *Feodosia pseudopoda* and *Koktebelia satura* are not parasitoids, we conducted feeding experiments with large diatom cells. Despite the ability of the *F. pseudopoda* strain Colp-S9 to feed on large diatoms, we never observed the formation of trophosomes inside the diatom frustules. At the same time, this strain demonstrated a variety of feeding strategies for different types of diatom prey. These differences are probably due to variations in the structure of diatom frustules and require further study. One of the largest diatoms that Colp-S9 was able to consume by swallowing was the triangular diatom *Licmophora* sp., which is up to 45 μm long. When consumed, *Licmophora* sp. frustules maintain their shape and do not shrink into a shapeless lump, as occurs for less silicified frustules of the diatom *Attheya* sp. Parts of the diatom protoplast are probably delivered into the predator cell through some wide openings in the diatom frustule (e.g., openings at the end of the setae or gaps between girdle bands). Strutted or labiate processes are too small to allow large parts of the protoplast to be transferred outside of diatom frustules. We never observed the formation of trophosomes inside the diatom. Thus, digestion should take place outside of the diatom frustule. The ability of Colp-S9 cells to consume diatoms significantly larger than themselves is not unique in stramenopiles. For example, *Paraphysomonas* sp. can swallow diatom prey up to 10 times larger (Suttle et al., 1986).

The feeding strategy of Colp-S9 on two other large diatoms, *Coscinodiscus radiatus* and cf. *Pinnularia* sp., was apparently different. Predators attach to diatom frustules and release a wide pseudopodium, which is reminiscent of the attachment mechanism of the parasitoid *Pirsonia*. However, this pseudopodium penetrates through some holes and transports parts of diatom protoplast and individual chloroplasts to the main cell part of the predator without formation of a trophosome inside the frustule. The food vacuole is formed in this main part of the predator cell (Figure 4O-Q), which is a major difference from parasitoid behavior, where digestion occurs in the trophosome, outside the main body of the parasite. Frustule holes, the nature of which is unclear, should be wide enough to allow parts of diatom protoplasts and even individual chloroplasts to pass through. They may be less silicified parts of the cingulum, possibly during the diatom division process when the cingulum becomes vulnerable, or some frustule damages. This is confirmed by the fact that less than half of the diatom cells were consumed in culture. Interestingly, Colp-S9 was not able to consume many other large diatom species.

Another marked difference in feeding on large diatoms between Colp-S9 and the parasitoid *Pirsonia* is that predators maintain full-length and actively beating flagella, thus continuing to swim. The flagella of the parasitoid *Pirsonia* always retract during infection, except *P. eucampiae*, whose flagella are only partially retracted (Kühn et al., 1996). Likewise, when Colp-S9 forms multiflagellated cells through multiple sequential incomplete cell divisions, daughter flagellates remain active and determine the movement of the entire organism. On the other hand, some resting cells of *Noirmoutieria diatomophaga* shed their flagella, resulting in non-flagellated round or irregular amoeboid cells resembling auxosomes, as was noted for eukaryotrophic Pirsoniales (Cho et al., 2022).

It is important to note that parasitoid *Pirsonia* species also demonstrate variability in feeding mechanisms. For example, *P. diadema* and *P. punctigerae* use only strutted processes to enter diatom frustules, while *P. guinardiae* can also use the overlap between the two valvae in the girdle region, and *P. punctigerae* sometimes uses large areolae in the center of the valvae (Schweikert and Schnepf, 1997). When most *Pirsonia* species feed, the host cytoplasm migrates to the site of infection (Kühn et al., 1996; Scnepf et al., 1990), whereas when infected by *P. punctigerae*, the host cytoplasm moves in the opposite direction (Schweikert and Schnepf, 1997). On the basis of the limited studies available, most *Pirsonia* species appear to be host-specific (Table S2), with the exception of *P. formosa*, which is able to infect up to nine diatom species (Kühn et al., 1996, 2004). Little is known about the feeding strategies of *P. formosa* in relation to its diverse hosts. One possible example of adaptation to parasites on different diatom species is the ability to infect different life stages of the hosts (vegetative cells, dormant spores or naked protoplasts only) (Kühn et al., 1996, 2004). It is also known that the size of the infected diatom determines the growth of the parasite (the larger the host cell is, the greater the number of parasite cell divisions).

Morphological features of Pirsoniales and comparison with related groups

The presence of a ventral groove interspersed with a protrusion of the flagella emergence site is a common morphological feature of all Pirsoniales. This feature differentiates them from the sister group Developea. Although developeans have a ventral depression that is homologous to a groove, they lack a protrusion dividing it into anterior and posterior parts. Unlike in Pirsoniales, where flagella emerge from the ventral protrusion, flagella of developeans emerge from the bottom of the anterior part of the ventral depression (Aleoshin et al., 2016; Cho et al., 2022; Tong, 1995; Weiler et al., 2021). The ventral groove of developeans is not divided into anterior and posterior parts. Thus, the body plane of Pirsoniales is more similar to that of oomycete zoospores, which have well-defined ventral grooves and prominent protrusions (Ho et al., 1968; Lunney and Bland, 1976).

The ventral groove is widespread in stramenopiles. In addition to Bigyromonadea and oomycetes, it is found in in labyrinthulomycetes (Barr and Allan, 1985), *Kaonashia insperata* (Weston et al., 2023), *Platysulcus tardus* (Shiratori et al., 2015; Thakur et al., 2019), and a likely homologous structure is present also in bicosoecids and placidideans (Moriya et al., 2000, 2002; O'Kelly and Patterson, 1996; Teal, 1998). Outside the stramenopiles, the ventral groove can be found in many diverse eukaryotic groups: jakobids, most metamonads and malawimonadids (Simpson, 2003), alveolates (Tikhonenkov et al., 2014), rhizarians (Howe et al., 2011), provorans (Tikhonenkov et al., 2022), and collodictyonids (Brugerolle, 2006; Brugerolle et al., 2002). This structure is always supported by elements of an extremely conserved flagellar apparatus and is thus considered an ancestral structure for all eukaryotes (Cavalier-Smith, 1978; Yubuki and Leander, 2013). Identifying and studying this structure in new taxonomic groups further supports the adaptive importance of this trait and its likely occurrence in the last eukaryotic common ancestor.

We observed pseudopodia in all our strains. In parasitoid *Pirsonia*, pseudopodia play an important role in feeding due to their involvement in frustule invasion and trophosome formation (Schnepf and Schweikert, 1997; Schweikert and Schnepf, 1997). In predatory Pirsoniales, which do not possess any specialized cellular structure for nutrition, such as a cytostome, pseudopodia also play a role in feeding. Sometimes, they are also used for temporary substrate attachment. In the resting cells of *Koktebelia satura*, we observed the release of pseudopodia of unknown function. An interesting observation was made on starved *Pirsonia punctigera* cells, which became motionless, settled on the substrate and formed long filopodia-like processes in contact with each other (Schweikert and Schnepf, 1997). This is reminiscent of the formation of an ectoplasmic network in labyrinthulomycetes (Anderson and

Cavalier-Smith, 2012; Gomaa et al., 2013; Iwata et al., 2016), which possess amoeboid stages in the life cycles and rhizopoda-like structures (Anderson and Cavalier-Smith, 2012; Benneth et al., 2017; Gomaa et al., 2013; Takahashi et al., 2014). It is known that the trophosomes of different *Pirsonia* cells may fuse inside the cell of the same diatom during multiple infections (Kühn et al., 1996). Apparently, similar amoeboid features unite labyrinthulomycetes and Pseudofungi and were present ancestrally before the divergence of these groups.

The species *Feodosia pseudopoda* is capable of forming large multinucleated and multiflagellated cells. This could be a single large oval cell with two, four, etc., nuclei and associated sets of flagella, as illustrated by Hoechst staining (Figure 10). Such structures represent compact multinucleated forms that can be considered as predecessors of multicellularity (Lamża, 2023). Sometimes cells undergo several consecutive incomplete cell divisions without complete separation, thus forming temporary colonies of independent cells that are attached to each other and usually to a large common food vacuole by long posterior protrusions. The formation of these facultative colonies occurs in the presence of a large amount of food (diatoms) and disappear gradually as the amount of diatom prey decreases. It remains unclear what causes the formation of compact multinucleated cells and what they subsequently transform into; whether into individual cells or into temporary colonies. The question is also whether this process is related to sexual reproduction. A detailed study of the life cycle of *F. pseudopoda* is needed to address these questions.

The formation of facultative colonies in *F. pseudopoda* is likely related to the formation of auxosome-type colonies in parasitic Pirsoniales. Both phenomena are limited by the amount of food available. The formation of a large common food vacuole filled with brownish material of undigested diatom shells and chloroplasts in *F. pseudopoda* is reminiscent of trophosome formation in parasitoid *Pirsonia* species (Schnepf and Schweikert, 1997; Schweikert and Schnepf, 1997). Such food vacuoles may be up to 20 times larger than a single diatom cell. The presence of both facultative colonies and large shared accumulative food vacuoles observed in *F. pseudopoda* suggests that they may represent ancestral characteristics of all Pirsoniales that contributed to the development of parasitism in the *Pirsonia* clade.

Another remarkable feature of the novel *F. pseudopoda* strain KT49-10a is its ability to self-aggregate with possible cell fusion, which differs from the colonial formation resulting from cell division. This is the first observation of self-aggregation in Pirsoniales. Individual cells, probably attracted by chemical signals, join to form a common pellet of cells that are pressed tightly to each other (Figure 4U). This behavior is likely initiated by starvation-induced stress. Self-aggregation is a very rare phenomenon well known to occur in oomycete zoospores (Bassani et al., 2020; Ko and Chase, 1973; Reid et al., 1995; West et al., 2003) and recently detected in developeans (Cho et al., 2022). The discovery of this feature in Pirsoniales suggests that it is a very likely ancestral character of Pseudofungi. We also frequently observed loose clusters of aggregated cells in starved cultures of *Koktebelia satura* without cell fusion. Similar behavior was noted for the parasitoid *Pirsonia guinardiae*, which assembles on the inner surface of empty diatom frustules in starved cultures (Kühn et al., 1996). Interestingly, all three documented self-aggregation behaviors in Pirsoniales are related to starvation.

Chemotaxis is likely involved in self-aggregation of oomycete zoospores (Bassani et al., 2020; Reid et al., 1995), as it is involved in their aggregation on plants. It is assumed that this may occur due to the release of certain chemicals by the zoospores themselves, which increases the likelihood of infection due to the lack of stimulation from the host (Savoty et al., 2014). Genomic and transcriptomic studies of oomycetes have revealed the presence of proteins associated with the adhesion and signaling homologous to those required for the multicellular development of metazoans and their closest protist relatives (Bassani et al., 2020; King et al., 2003, 2008; Sebé-Pedrós et al., 2013). For example, a whole family of oomycete-specific cadherins has been discovered (Fletcher et al., 2016). Cadherins are also involved in

cell adhesion and aggregation in *Dictyostelium* (Hulpiau et al., 2013; Niklas and Newman, 2013). The developing auxosomes and newly-formed flagellated cells of *Pirsonia* are held together by a layer of mucilage, which is noticeable only via SEM (Schweikert and Schnepf, 1997). Our SEM observation revealed similar coverage of individual cells of pirsoniales (Figure 2). Further genomic and transcriptomic studies of these organisms, together with ultrastructural observations of amoeboid and aggregative stages, will help to elucidate the nature and mechanisms of self-aggregation in this group, as well as the relatedness of this phenomenon to self-aggregation in oomycetes.

We did not find cysts in our cultures, although all studied strains had resting cells that retained flagella (except for the species *Noirmoutieria diatomophaga*) and that varied in shape, from non-flattened ovals with preserved ventral groove to rounded or irregularly amoeboid and flattened ones. Among *Pirsonia* species, round cysts with red-brown or dark brown walls filled with refractive granules, are found only in *P. guinardiae* (Schnepf et al., 1990). These cysts appear to be true resting cysts, in contrast with the resting cells we observed.

Ultrastructure of the novel Pirsoniales

The ultrastructure of the new strains is very similar to that of known *Pirsonia* species (Schnepf and Schweikert, 1997; Schweikert and Schnepf, 1997). All cells we studied were covered with hair-like structures, similar to the hairs covering the posterior flagellum. Similar structures, named as knotted body hairs, have been found in *Pirsonia* (Schweikert and Schnepf, 1997). However, the length of the hair-like structures we observed was twice shorter, 0.2-0.25 µm vs. 0.4-0.5 µm in *Pirsonia* (Schnepf and Schweikert, 1997; Schweikert and Schnepf, 1997), although previous observations were based on whole mount TEM. In contrast to our species, body hairs in *Pirsonia* appear only at certain life cycle stages. In particular, life cycle stages associated with parasitism, such as auxosomes, developing flagellated cells, and flagellated cells before attachment to diatoms, lack body hairs (Schnepf and Schweikert, 1997; Schweikert and Schnepf, 1997). It is expected that we would observe hair-like structures on all studied cells since the novel predatory Pirsoniales do not have life cycle stages associated with parasitism (see above). These hair-like structures are specific to the order Pirsoniales since they have not been observed in other stramenopiles (Aleoshin et al., 2016; Beakes and Thines, 2017; Bennett et al., 2017; Kristiansen and Škaloud, 2017; Shiratori et al., 2015, 2017; Thakur et al., 2019; Tong, 1995; Weston et al., 2023). The structure and role of these hair-like structures in Pirsoniales need to be studied.

Different types of cell body hairs, somatonemes, cover the posterior half of the cell of the flagellate *Proteromonas lacerate* (Opalozoa, Stramenopiles), a tetrapod gut commensal (Brugerolle and Bardele, 1988). Somatonemes are very similar to mastigonemes: they are also tubular and tripartite and are synthesized in the ER cisternae. Additionally, somatonemes are anchored to cortical microtubules in the same way that mastigonemes are anchored to axonemal microtubules (Brugerolle and Bardele, 1988). Somatonemes probably evolved to adapt to an endobiotic habitat and transition from phagocytosis to pinocytosis by protecting cells from large and sharp food particles that can stick to the cell and interfere with pinocytosis, as well as damage the cell surface (Cavalier-Smith, 1998). Further studies will help to investigate the evolutionary relationship between both types of hair-like structures and whether these structures have a common evolutionary origin or have arisen independently.

The known parasitoid *Pirsonia* has a spherical nucleus, as we observed in two of three of our species (*Bullionia fluviatilis* and *Feodosia pseudopoda*). By contrast, the nucleus of *Bordeauxia parva* is elongated pear-shaped, similar to the nuclei of most stramenopiles, including developeans, oomycetes, hyphochytriomycetes, labyrinthulomycetes, many opalozoans and some ochrophytes (Aleoshin et al., 2016; Barr, 1981; Barr and Allan, 1985; Gotelli and Hanson, 1987; Hardham, 1987; Lunney and Bland, 1976; Maistro et al., 2017;

Moriya et al., 2000; 2002; Tong, 1995). A spherical nucleus with eccentrical nucleolus has been observed in young oomycete zoospores released from sporangia (Lunney and Bland, 1976). Like the parasitoid *Pirsonia*, all our species have two nuclear papillae (protrusions) from the side of the nucleus located closer to the kinetosomes. Such nuclear papillae are not known even for the closely related developeans and are likely a characteristic feature of the order Pirsoniales. These papillae serve to attach the nucleus to the posterior kinetosome.

The cytoplasm of our new species contains diverse round and flattened vesicles, microbodies, multivesicular bodies, and lipid droplets. We found large and roundish vesicles, not necessarily associated with the cell periphery, in *Feodosia pseudopoda*, while flattened vesicles in *Bordeauxia parva* always underlay the plasmalemma. Different types of vesicles are found in many stramenopile groups. Flattened cortical vesicles in *B. parva* resemble those found in developeans (Aleoshin et al., 2016; Tong, 1995) and *Kaonashia insperata* (Weston et al., 2023). A single large flat vesicle surrounds the cytoplasm with the nucleus, mitochondria, and microbodies in the cells of *Platysulcus tardus* (Shiratori et al., 2015). Large round peripheral vesicles are also found in *Pseudophyllomitus vesiculosus* (Shiratori et al., 2017). In *K. insperata*, flattened vesicles are intermitted by extrusomes; in developeans, they are intermitted by densely stained bodies. Interestingly, both hyphochytrid and oomycete zoospores have several types of peripheral vesicles, including very thin peripheral cysternae and densely stained vesicles involved in adhesion and incorporation into the cyst coat (Beakes et al., 2014). It remains unclear whether such structures are homologous to cortical vesicles and densely stained bodies in developeans and Pirsoniales.

The kinetosomal structure, and especially the transitional zone of kinetosomes, is considered an extremely important morphological structure to study phylogenetic relationships (Cavalier-Smith, 2022; Manton, 1964). The kinetosome structure is similar in all our studied strains and corresponds to that of known *Pirsonia* species (Schnepf and Schweikert, 1997; Schweikert and Schnepf, 1997). However, the transitional zone of *Pirsonia* was not described in detail. It is very difficult to obtain good images of pirsonial kinetosomes with attached flagella, as they tend to detach during fixation. The transitional zone of flagella of our studied species possesses a single transitional helix with 3-6 gyres, as described for *Pirsonia* (Schnepf and Schweikert, 1997; Schweikert and Schnepf, 1997). In general, transitional helices are widely present in stramenopiles and are extremely rare outside this group, being their characteristic feature (Thakur et al., 2019). In addition to Pirsoniales, single transitional helices are present in most ochrophytes (Andersen, 2004) and *Pseudophyllomitus vesiculosus* (Shiratori et al., 2017). A double helix is known in developeans (Tong, 1995), hyphochytriomycetes and most oomycetes (Barr, 1981; Barr and Allan, 1985; Barr et al., 1985; Beakes and Thines, 2017; Beakes et al., 2012, 2014), Placididea (Moriya et al., 2000, 2002), and ochrophyte Xanthophyceae (Andersen, 2004). Most bicosoecids, some ochrophytes (Bolidophyceae, diatoms, Phaeophyceae, and Raphidophyceae) and *Platysulcus tardus* have lost this structure (Andersen, 2004; Cavalier-Smith and Chao, 2006; Karpov et al., 2001; O'Kelly and Patterson, 1996; Preisig, 1989; Shiratori et al., 2015; Teal et al., 1998; Yubuki et al., 2010), while labyrinthulomycetes have similarly placed cone-like structures (Bennett et al., 2017). The double helix in the transition zone of the flagellum, as the most common type, is considered the ancestral feature for stramenopiles (Thakur et al., 2019), however, such a structure may be modified in closely related groups. The transitional zone of our new strains also contained a transverse plate and annular connections, both located almost at the same level. These structures are well-known for stramenopiles and other eukaryotes (Cavalier-Smith, 2022). Electron-dense central thickening of the transverse plate is sometimes visible on some sections. Acorn-V system, recognized by Cavalier-Smith (2022) in stramenopiles for the first time, is probably present in all studied strains, but it is difficult to notice. It is visible as thin transverse filaments on longitudinal sections of *Feodosia*, just above central dense hub (Figure

8), and as lattice structure on transverse sections of *Bullionia*, immediately after the transition from triplets to doublets (Figure 9G).

We have observed a difference between parasitoid and predatory Pirsoniales in the orientation of the kinetosomes relative to each other. In parasitoid *Pirsonia* species, they diverge at a right angle (Schnepf and Schweikert, 1997; Schweikert and Schnepf, 1997) whereas in our new predatory strains they are oriented at a wide angle. In the closely related developeans, this angle ranges between 60° and 120° (Aleoshin et al., 2016; Tong, 1995) and depends on the type of cell, swimming or feeding ones (Aleoshin et al., 2016). A wide angle between kinetosomes is common in zoospores of oomycetes (Barr and Allan, 1985; Gotelli and Hanson, 1987; Lunney and Bland, 1976; Randolph and Powell, 1992) and hyphochytriomycetes (Barr, 1981; Barr and Allan, 1985). Deep branching stramenopiles and ochrophytes mostly have right or narrow angles between kinetosomes (Andersen, 2004; Honda and Inouye, 1995; Iwata et al., 2017; Kristiansen and Walne, 1977; Moriya et al., 2000, 2002; Mylnikov et al., 2008; O'Kelly and Patterson, 1996; Owen et al., 1990; Shiratori et al., 2015, 2017; Teal et al., 1998; Yubuki et al., 2010).

Here we need to note that anterior and posterior kinetosomes were probably mixed up in previous studies of Pirsoniales (Schnepf and Schweikert, 1997; Schweikert and Schnepf, 1997). They are difficult to identify on thin sections since obtaining well-fixed preparations for TEM is problematic and the flagella almost always detach during fixation. During fixation, Pirsoniales do not retain clear outlines of cell body shape and do not have a clear localization of most cell compartments. The ventral groove is not always pronounced, and kinetosomes are located halfway along the ventral groove, making it difficult to identify the anterior and posterior parts of the cell. According to the TEM images on Figures 20 and 21 from Schnepf and Schweikert (1997), the proximal end of the anterior kinetosome (with a distinctive cartwheel structure) is directed toward the side of the posterior kinetosome. By contrast, new Pirsoniales strains, as well as other studied stramenopile groups, having the opposite configuration, i.e. the proximal end of the posterior kinetosome is directed toward the side of the anterior kinetosome (Barr and Allan, 1985; Beakes et al., 2014; Iwata et al., 2017; Owen et al., 1990; Shiratori et al., 2015, 2017; Tong, 1995). In addition, the schematic illustration of the flagellar apparatus in Figure 27 from Schnepf and Schweikert (1997) contradicts to their own TEM illustrations and goes in accordance with 'canonical' stramenopile kinetosome connection. Also, according to our observations, the posterior kinetosome is connected to the nucleus by nuclear bands (Figures 6B, 8G,H, 9H-J), while previous descriptions of parasitic *Pirsonia* referred to the anterior kinetosome (Schnepf and Schweikert, 1997). In this case, we are confident that the nuclear bands extend from the posterior kinetosome on the basis of the associated posterior root R2 with the characteristic semicircular orientation of its microtubules (Figures 6B, 8G,H, 9H-J).

In all known Pirsoniales, the kinetosomes are connected to each other by two fibrillar bands: a short and wide proximal striated connecting band and a long and thin distal connecting band (Schnepf and Schweikert, 1997; Schweikert and Schnepf, 1997). These bands may be present in developeans but have not been studied in detail (Aleoshin et al., 2016; Tong, 1995). The dorsal connecting band is probably visible in Figure 15 (Tong, 1995) and in Figures 3C,D,F-H (Aleoshin et al., 2016). The proximal striated band and its modifications have been found in diverse stramenopile groups, such as a striated fan-shaped band in oomycetes (Barr and Allan, 1985; Gotelii and Hanson, 1987; Holloway and Heath, 1977; Lunney and Bland, 1976; Randolph and Powell, 1992) and two striated bands in bicosoecids and placidideans (Moriya et al., 2000, 2002; O'Kelly and Patterson, 1996; Teal et al., 1998). By contrast, the distal connecting band seems to be specific of Bigyromonada.

As mentioned before, the posterior kinetosome is connected to the nucleus by two electron-dense fibrous nuclear bands. These nuclear bands appear to be unique of Pirsoniales,

although homologous structures are likely present in oomycetes as a single striated strap extending from the posterior kinetosome along the surface of the nuclear envelope (Barr and Allan, 1985; Holloway and Heath, 1977; Randolph and Powell, 1992; Schnepf et al., 1978). Most ochrophytes are known to have a wide and prominent striated structure, the rhizoplast, connecting the anterior kinetosome with the nucleus, which is positioned at some distance from the kinetosomes (Andersen, 2004; Bouck and Brown, 1973; Kristiansen and Škaloud, 2017; Kristiansen and Walne, 1977; Owen et al., 1990).

The flagellar root system in our studied species is much more complex than that in known *Pirsonia* species and more similar to those of other stramenopiles. All four flagellar roots are microtubular in our strains, whereas only the roots associated with the posterior (indicated as "anterior" in Schnepf and Schweikert (1997)) kinetosome are microtubular in *Pirsonia* (Schnepf and Schweikert, 1997). Anterior (mentioned as "posterior" in Schnepf and Schweikert (1997)) roots in *Pirsonia* are fibrous, and posterior roots ("anterior" according to Schnepf and Schweikert (1997)) are highly reduced: four microtubules and a fibrillar band in root r1 and a single microtubule and several fibrillar bands in r2. However, Schnepf and Schweikert (1997) did not explain in detail the orientation of the roots in the cell, which makes it difficult to compare the roots of *Pirsonia* with the homologous roots in other eukaryotes (Moestrup, 2000; Yubuki and Leander, 2013). In most eukaryotes, the posterior root is more developed and is always associated with the ventral groove if such a structure is present (Yubuki and Leander, 2013). Therefore, it is more likely that the anterior root, not the posterior root, is reduced in *Pirsonia*. In any case, the flagellar root system of the parasitoid *Pirsonia* is reduced compared to that of other stramenopiles, which might be due to their parasitoid lifestyle. For example, some roots might be absent or poorly developed at some non-flagellated stages of the life cycle. This is consistent with the general trend of independent loss of complexity of the flagellar apparatus in some eukaryotic lineages during the transition from a free-living lifestyle to a symbiotic or parasitic lifestyle (Yubuki et al., 2016). These transitions are most likely related to changes in cell motility, attachment and nutrition. Well-known examples of microtubular reduction in parasitic lineages in comparison with their free-living relatives are slopalinids and *Blastocystis* (Stramenopiles), apicomplexans (Alveolates), diplomonads (Fornicata), and trypanosomatids (Euglenozoa) (Yubuki et al., 2016).

The most conspicuous right posterior root, r2, has 8-9 microtubules that are oriented in semicircle in its proximal part and reinforced with fibrous core material inside the semicircle. The same structure of the proximal part of r2 (U-shaped or L-shaped, which can be considered a modification of a semicircle) is present in most stramenopiles, e.g., developeans (Aleoshin et al., 2016; Tong, 1995), labyrinthulomycetes (Kazama, 1972, 1980; Perkins, 1974), *Pseudophyllomitus vesiculosus* (Shiratori et al., 2017), opalozoans (Moriya et al., 2000, 2002; O'Kelly and Patterson, 1996; Teal et al., 1998), *Platysulcus tardus* (Shiratori et al., 2015), and ochrophytes (Andersen, 2004; Honda and Inouye, 1995; Mylnikov et al., 2008; Owen et al., 1990). Oomycetes differ by having a flat arrangement of microtubules in r2 (Barr, 1981; Barr and Allan, 1985; Gotelli and Hanson, 1987; Randolph and Powell, 1992), and hyphochytriomycetes have greatly reduced r2 due to the loss of the second flagellum (Barr, 1981; Barr and Allan, 1985; Beakes and Thines, 2017). The fibrous material supporting this root from inside the semicircle and connecting it to the posterior or to both kinetosomes is also widely present in stramenopiles, e.g., fibrous core material inside the semicircle in developeans and placidideans (Aleoshin et al., 2016; Moriya et al., 2000; Tong, 1995), electron-dense backing material in labyrinthulomycetes (Kazama, 1972, 1980; Barr, 1981; Perkins, 1974), a striated band in bicosoecids (O'Kelly and Patterson, 1996; Teal et al., 1998; Yubuki et al., 2010), multilayered buttress in oomycetes (Barr, 1981; Barr and Allan, 1985; Gotelli and Hanson, 1987; Randolph and Powell, 1992; Holloway and Heath, 1977), and fibrous material in ochrophytes (Andersen, 2004; Owen et al., 1990; Mylnikov et al., 2008).

The left posterior root r1 in the new Pirsoniales species possesses a larger number of microtubules (3-5) compared with those (1-2) in other stramenopile groups (Aleoshin et al., 2016; Andersen, 2004; Barr, 1981; Barr and Allan, 1985; Gotelli and Hanson, 1987; Moriya et al., 2000, 2002; Owen et al., 1990; Randolph and Powell, 1992; Shiratori et al., 2015). A similar number of microtubules (3-4) was found only in Platysulcea, (Shiratori et al., 2015). The root r1 is absent in hyphochytriomycetes (Beakes and Thines, 2017) and in some ochrophytes (Andersen, 2004).

The right anterior root r3 of the novel Pirsoniales was also more similar to that of most stramenopiles than to *Pirsonia* in terms of its ribbed structure (the presence of secondary microtubules emerging at the right angle from the main microtubules) and in its clockwise direction. Secondary microtubules run anterior-dorsally and support the anterior part of the cell. The same structure (ribbed r3 with 2-3 main microtubules) is present in most stramenopiles (Aleoshin et al., 2016; Andersen, 2004; Barr, 1981; Barr and Allan, 1985; Gotelii and Hanson, 1987; Holloway and Heath, 1977; Iwata et al., 2017; Moriya et al., 2002; O'Kelly and Patterson, 1996; Randolph and Powell, 1992). Apparently, secondary microtubules are absent in Eustigmatophyceae, *Platysulcus*, *Pseudophyllomitus* and *Wobblia lunata* (Andersen, 2004; Moriya et al., 2000; Shiratori et al., 2015, 2017). In oomycetes, r3 is also strengthened with osmiophilic material along its way (Barr, 1981; Barr and Allan, 1985; Gotelii and Hanson, 1987; Holloway and Heath, 1977; Randolph and Powell, 1992).

The most inconspicuous left anterior root, r4, contains 1-2 microtubules, as in many stramenopiles (Andersen, 2004; Barr, 1981; Barr and Allan, 1985; Gotelli and Hanson, 1987; Iwata et al., 2017; Moriya et al., 2000, 2002; O'Kelly and Patterson, 1996; Shiratori et al., 2015, 2017; Teal et al., 1998).

The cytoplasmic and nuclear microtubules that we observed are common for many stramenopile groups (Barr, 1981; Barr and Allan, 1985; Gotelli and Hanson, 1987; Randolph and Powell, 1992; Holloway and Heath, 1977; Moriya et al., 2002; O'Kelly and Patterson, 1996; Teal et al., 1998; Andersen, 2004). Notably, such cytoplasmic microtubules are difficult to detect in thin sections (Barr, 1981; Barr and Allan, 1985).

Taxonomy, phylogeny and evolution

We identified five new genera in the order Pirsoniales, which indicates that this group of eukaryotes remains poorly studied in terms of its taxonomic diversity. Two of the studied Pirsoniales (*Feodosia pseudopoda* and *Koktebelia satura*) were described previously under provisional names because the obtained data were insufficient to describe new genera and species (Cho et al., 2022). Here, we studied their biology and morphology, which allowed us to formally describe them. We keep the provisional names proposed for these taxa in their taxonomic descriptions to avoid further confusion (see the taxonomic summary).

The 18S rRNA phylogenetic trees clarified the position of the novel strains within Pirsoniales and their relationships with already known parasitoid and predatory protists and environmental sequences. According to these results, close environmental lineages exist for almost all new Pirsoniales, except for *Feodosia* (Figure S1). Further research efforts should be directed to find and investigate these lineages, as well as to a more extensive survey of current metabarcoding datasets to explore the distribution of Pirsoniales. The largest number of lineages identified by environmental sequencing corresponds to the *Noirmoutieria* clade. Interestingly, they are all associated with anoxic or oxygen-limited habitats. A study of the tolerance of *Noirmoutieria* to low-oxygen conditions would be useful when the culture is reisolated.

We also identified the first freshwater representative of the Pirsoniales clade, which likely had an ancestor of marine origin. The transition of *Bullionia fluviatilis* to freshwater ecosystems probably occurred early in the evolution of Pirsoniales, but poor phylogenetic

support and more thorough sampling hinder the interpretation of this eco-evolutionary scenario.

The genera *Pirsonia* and *Noirmoutieria* constitute the family Pirsoniaceae. Concerning the other genera within the order Pirsoniales, the topology of our 18S rRNA phylogenetic tree, highly or moderately supported depending on the branch, is not necessarily consistent with the results of previous phylogenomic analyses (Cho et al., 2022, 2024). This is likely due to the limited information from this single marker, although differential taxon sampling can also have an effect. Therefore, we refrain from describing new families at this stage; they should be defined in subsequent studies using more in-depth phylogenomic data. This will help to clarify the relationships between the main clades of Pirsoniales and also to verify the monophyly of Bigyromonadea and their position within Stramenopiles. Molecular phylogenetic studies of small heterotrophic groups, such as Pirsoniales and Developea, can impact our interpretation of the evolution of large and important groups, such as oomycetes and ochrophytes. If Bigyromonadea are sister to oomycetes, as shown in previous studies (Cavalier-Smith and Chao, 2006; Cho et al., 2022, 2024; Noguchi et al., 2016; Thakur et al., 2019), this will help to reconstruct the ancestral state of oomycetes and advance our understanding of the origins of parasitism in this economically important group.

Alternatively, the possible relationship of Bigyromonadea with ochrophytes, as shown in a number of earlier studies (Aleoshin et al., 2016; Cho et al., 2022, 2024; Kühn et al., 1996; Leonard et al., 2018) also looks intriguing and, if confirmed, could help to understand the processes underlying the acquisition of plastids in one of the most important group of photosynthetic eukaryotes of planetary-scale ecological significance. Previously, mostly bacteriotrophic species were known for being closely related to ochrophytes (Aleoshin et al., 2016). However, further research demonstrated that eukaryotrophic protists are commonly found at the base of the most important stramenopile lineages (Aleoshin et al., 2016; Cho et al., 2022, 2024; Weston et al., 2023). Our finding of the ability of new Pirsoniales to successfully consume red algae is particularly intriguing given the rhodophyte ancestry of the ochrophyte plastids (Yoon et al., 2002). Red algae are considered unsuitable prey for most predators due to their thick polysaccharides and glycoprotein cell wall that serves to protect against recognition as prey and digestion (Martel, 2009; Ucko et al., 1997, 1999;). Therefore, the discovery of protists in natural ecosystems that can consume red algae and that branch close to ochrophytes is very relevant from an evolutionary point of view.

CONCLUSIONS

The identification and morphological and phylogenetic study of new members of the order Pirsoniales, including the first freshwater species, resulted in the description of five new genera and the emendation of the diagnosis of the order, previously known to be parasitic, as it now contains also predatory flagellates.

The formation of multiflagellated cells with a common large food vacuole, which is found in *Feodosia pseudopoda*, is reminiscent of trophosome and auxosome formation in *Pirsonia* and suggests its preparasitic origin. We observed self-aggregation in Pirsoniales for the first time and propose that this trait was present in the common ancestor of Pseudofungi. Our new species illustrate the astonishing diversity of strategies evolved in the order Pirsoniales for the effective consumption of diatoms, including parasitism with the formation of trophosomes and auxosomes, predation via the capture of whole cells, or via the use of pseudopodia to absorb/scavenge parts of protoplasts and chloroplasts through holes in the frustules.

The ultrastructure of the new strains shows that they share more features in the flagellar apparatus with other stramenopiles than with the known *Pirsonia* species. These features

include four microtubular roots, an arrangement of r2 microtubules in a semicircle and its division into two parallel rows, a ribbed r3 backed with fibrous material, and the orientation of kinetosomes. Hair-like structures covering the cell body and two nuclear bands connecting the nucleus with the posterior kinetosome are unique structures for the order Pirsoniales that define this taxon. Our results provide further support for the similarity of Bigyromonadea cells and oomycete zoospores, including new ultrastructural traits, such as general cell structure, orientation of kinetosomes relative to each other and the nucleus, direction of flagellar roots and the number of microtubules they contain.

Taxonomic summary

Zoobank Registration for this publication: urn:lsid:zoobank.org:pub:D320D0CD-FBC0-493C-8F6C-CBC4C5328BEF.

Taxonomy: Eukaryota; Sar; Stramenopiles; Gyrista; Bigyromonadea.

Order Pirsoniales Cavalier-Smith, 1998 emend.

Emended diagnosis: Biflagellated parasitoids of diatoms and eukaryotrophic predators. Parasitoid species differentiate into an intracellular feeding part (trophosome) and an external generative part (auxosome). With non-tubular hair-like structures on the cell body. Longitudinal ventral groove divided in anterior and posterior parts intermitted by a protrusion from which flagella emerge. Tubular mitochondrial cristae with a filament inside each crista. Kinetosomes connected to each other by a proximal striated connecting band and a distal connecting band. Posterior kinetosome connected with the nucleus by two nuclear bands. Transition zone of the flagellum contains a single helix above the transverse plate.

Family Pirsoniaceae Cavalier-Smith, 1998 emend.

Emended diagnosis: Biflagellated parasitoids of diatoms and eukaryotrophic predators. Parasitic species differentiate into an intracellular feeding part (trophosome) and an external generative part (auxosome). Round nucleus. Kinetosomes oriented at right angles to each other. Posterior kinetosome connected to the nucleus by a nuclear connecting band. Roots of posterior kinetosome are fibrillar (non-microtubular). Cells are covered with hair-like structures only at some life cycle stages. Cysts present in some species.

Type genus: *Pirsonia* Schnepf et al., 1990.

***Noirmoutieria* gen. nov.**

Diagnosis: Predators consuming heterotrophic flagellates and diatom algae. Elongated cells with well-developed longitudinal ventral groove. Oval, round, or irregular resting cells rarely shed flagella.

Etymology: Genus name reflects the source of the isolate, Noirmoutier-en-l'Île, France.

Zoobank Registration: urn:lsid:zoobank.org:act:34AD0014-5CA4-47E8-998E-DC7489442F4D.

Type species: *Noirmoutieria diatomophaga*

***Noirmoutieria diatomophaga* sp. nov.**

Diagnosis: Same as for the genus.

Type figure: Figure 3U illustrates a live cell of strain Pirs-sm2.

Type locality: Marine sediments of Noirmoutier-en-l'Île, France.

Etymology: Species named after its feeding mechanism, ability to swallow diatom cells.

Gene sequence: The 18S rRNA gene sequence has the GenBank Accession Number PP808839.

Zoobank Registration: urn:lsid:zoobank.org:act:4924A885-A9E4-4D6E-BD54-C582F61D5C09.

***Feodosia* gen. nov.**

Diagnosis: Eukaryotrophic predators. Round nucleus with small nuclear papillae. Slightly acentric nucleolus. Transitional helix in flagellum transition zone with 3-5 gyres. Large and round peripheral vesicles and flattened vesicles around the nucleus. Long and narrow nuclear bands. Presence of facultative multiflagellated colonial life cycle stages. Able to self-aggregate.

Etymology: Genus name kept as provisional from Cho et al. (2022) and reflects the source of isolate, the settlement Beregovoye, Feodosiya, Crimea.

Zoobank Registration: urn:lsid:zoobank.org:act:20F4AC14-1E06-4F44-A9A6-5B4208248795.

Type species: *Feodosia pseudopoda*

***Feodosia pseudopoda* sp. nov.**

Diagnosis: Same as for the genus.

Type figure: Figure 4A illustrates a live cell of strain NY0226.

Type culture: Strain NY0226 is deposited in the DEEM live culture collection, CNRS and Université Paris-Saclay (France).

Type material: A block of chemically fixed resin-embedded cells of the type strain, NY0226, is deposited in the DEEM culture collection, CNRS and Université Paris-Saclay (France). This constitutes the name-bearing type of the species (a hapantotype).

Type locality: Marine sediments of plage de Jean Blanc near Saint-Tropez, France.

Etymology: Species name kept as provisional from Cho et al. (2022) and reflects the ability to produce pseudopodia.

Gene sequence: The 18S rRNA gene sequence of the strain NY0226 has the GenBank Accession Number PP795933.

Zoobank Registration: urn:lsid:zoobank.org:act:DBB3C346-E4F1-404A-A47B-11C0BBA54778.

***Koktebelia* gen. nov.**

Diagnosis: Eukaryotrophic predators. Longitudinal ventral groove well developed. Resting cells are oval, with finger-like pseudopodia. Form clusters of resting cells in starved cultures.

Etymology: Genus name kept as provisional from Cho et al. (2022) and reflects the source of the isolate, Koktebel bay, Crimea.

Zoobank Registration: urn:lsid:zoobank.org:act:3D31C141-F8A9-4FA6-8228-30E7F7D7F4F0.

Type species: *Koktebelia satura*

***Koktebelia satura* sp. nov.**

Diagnosis: Same as for the genus.

Type figure: Figure 3N illustrates a live cell of strain Colp-Nor4.

Type culture: Strain Colp-Nor4 is deposited in the DEEM live culture collection, CNRS and Université Paris-Saclay (France).

Type locality: Marine sediments of Yport, France.

Etymology: Species name kept as provisional from Cho et al. (2022) and coming from satur (lat.), well-fed.

Gene sequence: The 18S rRNA gene sequence of the strain Colp-Nor4 has the GenBank Accession Number PP795565.

Zoobank Registration: urn:lsid:zoobank.org:act:8DD522CF-B652-43A7-A5D4-D3C640E8146D.

***Bordeauxia* gen. nov.**

Diagnosis: Eukaryotrophic predators. Longitudinal ventral groove poorly developed. Able to form thin pseudopodia. Pear-shaped nucleus with a narrowed part connected to kinetosomes by two nuclear bands. Flattened vesicles underlying plasmalemma. Transitional helix in flagellum transition zone with 3-5 gyres. Cytoplasmic microtubules originating from kinetosomes and conically radiating along the nucleus. Right posterior root r2 divided in two parallel rows in its middle part. Right anterior root r3 consists of three microtubules backed with fibrous material and perpendicularly oriented secondary microtubules. Left anterior root r4 consists of two microtubules and is oriented laterally.

Etymology: Genus name reflects the source of the isolate, Gironde estuary near Bordeaux, France.

Zoobank Registration: urn:lsid:zoobank.org:act:B85AC3F7-C518-4F59-8D16-B900B5CE10A3.

Type species: *Bordeauxia parva*

***Bordeauxia parva* sp. nov.**

Diagnosis: Same as for the genus.

Type figure: Fig. 3A illustrates a live cell of strain Colp-p1.

Type culture: Strain Colp-p1 is deposited in the DEEM live culture collection, CNRS and Université Paris-Saclay (France).

Type material: A block of chemically fixed resin-embedded cells of the type strain, Colp-p1, is deposited in the DEEM culture collection, CNRS and Université Paris-Saclay (France). This constitutes the name-bearing type of the new species (a hapantotype).

Type locality: Gironde estuary near Talmont-sur-Gironde, Nouvelle-Aquitaine, France.

Etymology: Species name means small in Latin.

Gene sequence: The 18S rRNA gene sequence of the strain Colp-p1 has the GenBank Accession Number PP808806.

Zoobank Registration: urn:lsid:zoobank.org:act:8DD70CA4-51F5-4ABE-A86A-B21DF7BD5743.

***Bullionia* gen. nov.**

Diagnosis: Eukaryotrophic predators. Longitudinal ventral groove poorly developed. Round or irregular nucleus with prominent nuclear papillae. Long striated nuclear bands. Slightly acentric nucleolus. Large reserve lipid droplets. Transition helix in flagellum transition zone with six gyres. Round flattened resting cells.

Etymology: Genus name reflects the source of the first isolate of this organism, near the town of Bullion, Ile-de-France, France.

Zoobank Registration: urn:lsid:zoobank.org:act:66362B67-A30D-4D0D-BCD2-AE7985F88A55.

Type species: *Bullionia fluviatilis*

***Bullionia fluviatilis* sp. nov.**

Diagnosis: Same as for the genus.

Type figure: Figure 3H illustrates a live cell of strain Pirs-vl.

Type culture: Strain Pirs-vl is deposited in the DEEM live culture collection, CNRS and Université Paris-Saclay (France).

Type material: A block of chemically fixed resin-embedded cells of the type strain, Pirs-vl, is deposited in the DEEM culture collection, CNRS and Université Paris-Saclay (France). This constitutes the name-bearing type of the new species (a hapantotype).

Type locality: Valmont river, Valmont, Normandie, France.

Etymology: Species name refers to freshwater habitat in a river.

Gene sequence: The 18S rRNA gene sequence of the strain Pirs-vl has the GenBank Accession Number PP808838.

Zoobank Registration: urn:lsid:zoobank.org:act:91FB4FE3-0833-48EF-BF5D-7E193B13EFC5.

ACKNOWLEDGMENTS

This work is supported by the European Research Council (ERC) Advanced Grant "Plast-Evol" (787904) and by the Tyumen Oblast within the framework of the project of the West Siberian Interregional Scientific and Educational Center No. 89-DON (2). The TEM work has benefited from Imagerie-Gif core facility supported by l'Agence Nationale de la Recherche (ANR-10-INBS-04/FranceBioImaging; ANR-11-IDEX-0003-02/ Saclay Plant Sciences). The authors greatly acknowledge the Multimodal Imaging Center Imaging Facility of the Institut Curie (CNRS UAR2016/ Inserm US43/ Institut Curie / Université Paris-Saclay) for the interpretation of the images of electron microscopy. The authors are grateful to Sergey A. Karpov for advice about ultrastructural analysis; Vasily V. Vishnyakov for help with diatom identification; Varsha Mathur and Benjamin Bailleul for providing diatom cultures; Nikita G. Eremeev, Vasily V. Vishnyakov, Ludwig Jardiller, Feriel Bouderka, Jazmin Blaz and Samuel O'Donnell for their help in sample collection.

REFERENCES

Aleoshin, V. V., Mylnikov, A. P., Mirzaeva, G. S., Mikhailov, K. V. & Karpov, S. A. 2016. Heterokont predator *Develorapax marinus* gen. et sp. nov. – a model of the ochrophyte ancestor. *Front. microbiol.*, 7, 1194. doi:10.3389/fmicb.2016.01194

Altschul, S. F., Gish, W., Miller, W., Myers, E. W. & Lipman, D. J. 1990. Basic local alignment search tool. *J. Mol. Biol.*, 215:403-410.

Anderson, O. R. & Cavalier-Smith, T. 2012. Ultrastructure of *Diplophrys parva*, a new small freshwater species, and a revised analysis of Labyrinthulea (Heterokonta). *Acta Protozool.*, 51:291-304.

Anderson, R. M. & May R. M. 1978. Regulation and stability of host-parasite population interactions: 1. Regulatory processes. *J. Anim. Ecol.*, 47:219-247.

Andersen R. A. 2004 Biology and systematics of heterokont and haptophyte algae. *Am. J. Bot.*, 91:1508-1522.

Barr, D. J. 1981. The phylogenetic and taxonomic implications of flagellar rootlet morphology among zoosporic fungi. *BioSystems*, 14(3-4):359-370.

Barr, D. J. & Allan, P. M. 1985. A comparison of the flagellar apparatus in *Phytophthora*, *Saprolegnia*, *Thraustochytrium*, and *Rhizidiomyces*. *Canad. J. Bot.*, 63(1):138-154.

Barr, D. J. S & Desaulniers, N. L. 1989. The flagellar apparatus of the oomycetes and hyphochytriomycetes. *In:* Green J. C., Leadbeater B. S. C. & Diver W. L. (ed.), The chromophyte algae: problems and perspectives. Clarendon Press, Oxford. 343-355.

Bassani, I., Rancurel, C., Pagnotta, S., Orange, F., Pons, N., Lebrigand, K., Panabières, F., Counillon, L., Noblin, X. & Galiana, E. 2020. Transcriptomic and ultrastructural signatures

of K+-induced aggregation in *Phytophthora parasitica* zoospores. *Microorganisms*, 8(7):1012. doi:10.3390/microorganisms8071012.

Beakes, G. W., Glockling, S. L. & Sekimoto, S. 2012. The evolutionary phylogeny of the oomycete "fungi". *Protoplasma*, 249:3-19.

Beakes, G. W. & Thines, M. 2017 Hyphochytriomycota and oomycota. *In:* Archibald, J, M., Simpson, A. G. B. & Slamovits, C. H. (ed.), Handbook of the Protists. 2nd ed. Springer, Cham. 435-505.

Bennett, R. M., Honda, D., Beakes, G. W. & Thines, M. 2017. Labyrinthulomycota. *In:* Archibald, J, M., Simpson, A. G. B. & Slamovits, C. H. (ed.), Handbook of the Protists. 2nd ed. Springer, Cham. 507-542.

Brugerolle, G. 2006. Description of a new freshwater heterotrophic flagellate *Sulcomonas lacustris* affiliated to the collodictyonids. *Acta protozool*., 45(2):175-182.

Brugerolle, G. & Bardele, C. F. 1988. Cortical cytoskeleton of the flagellate *Proteromonas lacertae*: interrelation between microtubules, membrane and somatonemes. *Protoplasma*, 142:46-54.

Brugerolle, G., Bricheux, G., Philippe, H. & Coffe, G. 2002. *Collodictyon triciliatum* and *Diphylleia rotans* (= *Aulacomonas submarina*) form a new family of flagellates (Collodictyonidae) with tubular mitochondrial cristae that is phylogenetically distant from other flagellate groups. *Protist*, 153(1):59-70.

Capella-Gutiérrez, S., Silla-Martínez, J. M. & Gabaldón, T. 2009. trimAl: a tool for automated alignment trimming in large-scale phylogenetic analyses. *Bioinformatics*, 25:1972-1973.

Cavalier-Smith, T. 1978. The evolutionary origin and phylogeny of microtubules, mitotic spindles and eukaryote flagella. *BioSystems*, 10(1-2):93-114.

Cavalier-Smith, T. 1998. A revised six-kingdom system of life. *Biol. Rev*., 73(3):203-266.

Cavalier-Smith, T. 2004. Only six kingdoms of life. *Proc. R. Soc. Lond. Series B: Biol. Sci*., 271(1545):1251-1262.

Cavalier-Smith, T. 2022. Ciliary transition zone evolution and the root of the eukaryote tree: implications for opisthokont origin and classification of kingdoms Protozoa, Plantae, and Fungi. *Protoplasma*, 259(3):487-593.

Cavalier-Smith, T. & Chao, E. E. 2006. Phylogeny and megasystematics of phagotrophic heterokonts (kingdom Chromista). *J. Mol. Evol*., 62:388-420.

Cavalier-Smith, T. & Scoble, J. M. 2013. Phylogeny of Heterokonta: *Incisomonas marina*, a uniciliate gliding opalozoan related to Solenicola (Nanomonadea), and evidence that Actinophryida evolved from raphidophytes. *Eur. J. Protistol*., 49(3):328-353.

Cho, A., Tikhonenkov, D. V., Hehenberger, E., Karnkowska, A., Mylnikov, A. P. & Keeling, P. J. 2022. Monophyly of diverse Bigyromonadea and their impact on phylogenomic relationships within stramenopiles. *Mol. Phyl. Evol*., 171, 107468. doi:10.1016/j.ympev.2022.107468.

Cho, A., Tikhonenkov, D. V., Lax, G., Prokina, K. I. & Keeling, P. J. 2024. Phylogenomic position of genetically diverse phagotrophic stramenopile flagellates in the sediment-associated MAST-6 lineage and a potentially halotolerant placididean. Mol. Phyl. Evol., 107964. doi:10.1016/j.ympev.2023.107964.

Derelle, R., López-García, P., Timpano, H. & Moreira, D. 2016. A phylogenomic framework to study the diversity and evolution of stramenopiles (= heterokonts). Mol. Biol. Evol., 33(11):2890-2898.

Eliáš, M., Amaral, R., Fawley, K. P., Fawley, M. W., Němcová, Y., Neustupa, J., Přibyl, P., Santos, L. M. A. & Ševčíková, T. 2017. Eustigmatophyceae. *In:* Archibald, J, M., Simpson, A. G. B. & Slamovits, C. H. (ed.), Handbook of the Protists. 2nd ed. Springer, Cham. 367- 406.

Fletcher, K. I. G., van West, P. & Gachon, C. M. M. 2016. Nonagonal cadherins: A new protein family found within the Stramenopiles. *Gene*, 593:64-75.

Gachon, C. M, Sime-Ngando, T., Strittmatter, M., Chambouvet, A. & Kim, G. H. 2010. Algal diseases: spotlight on a black box. *Trends Plant Sci*., 15(11):633-640.

Gaines, G. & Elbrächter, M. 1987. Heterotrophic nutrition. *In:* Taylor, F. J. R. (ed.), Biology of Dinoflagellates. Blackwell Scientific, Oxford. 224-268.

Gomaa, F., Mitchell, E. A. D., Lara, E. & Crandall, K. A. 2013. Amphitremida (Poche, 1913) is a new major, ubiquitous labyrinthulomycete clade. *PLoS One*, 8(1), e53046. doi:10.1371/journal.pone.0053046.

Gotelli, D. & Hanson, L. C. 1987. An ultrastructural investigation of the zoospore of *Sapromyces androgynus* (Oomycetes, Leptomitales). *Mycologia*, 79(5):745-752.

Guillard, R. R. L. & Ryther, J. H. 1962. Studies on marine phytoplanktonic diatoms. 1. *Cyclotella nana* Hustedt and *Detonula confervacea* (Cleve) Gran. *Can. J. Microbiol*., 8:229-239.

Hardham, A. R. 1987. Ultrastructure and serial section reconstruction of zoospores of the fungus *Phytophthora cinnamomi*. Exp. Mycol., 11(4):297-306.

Hesse, M., Kusel-Fetzmann, E. & Carniel, K. 1989. Life cycle and ultrastructure of *Ducellieria chodati* (Oomycetes). *Plant Syst. Evol.*, 165:1-15.

Hibberd D. J. 1979. The structure and phylogenetic significance of the flagellar transition region in the chlorophyll c-containing algae. *BioSystems*, 11:243-261.

Ho, H. H., Zachariah, K. & Hickman, C. J. 1968. The ultrastructure of zoospores of *Phytophthora megasperma* var. *sojae*. Canad. J. Bot., 46(1):37-41.

Howe, A. T., Bass, D., Scoble, J. M., Lewis, R., Vickerman, K., Arndt, H. & Cavalier-Smith, T. 2011. Novel cultured protists identify deep-branching environmental DNA clades of Cercozoa: new genera *Tremula*, *Micrometopion*, *Minimassisteria*, *Nudifila*, *Peregrinia*. *Protist*, 162(2):332-372.

Hulpiau, P., Gul, I. S. & van Roy, F. 2013. New insights into the evolution of metazoan cadherins and catenins. *Prog. Mol. Biol. Transl. Sci.*,116:71-94.

Iwata, I., Kimura, K., Tomaru, Y., Motomura, T., Koike, K., Koike, K. & Honda, D. 2017. Bothrosome formation in *Schizochytrium aggregatum* (Labyrinthulomycetes, Stramenopiles) during zoospore settlement. *Protist*, 168(2):206-219.

Katoh, K., Misawa, K., Kuma, K.I. & Miyata, T. 2002. MAFFT: a novel method for rapid multiple sequence alignment based on fast Fourier transform. *Nucleic Acids Res*., 30(14):3059-3066.

Katoh, K., Rozewicki, J. & Yamada, K. D. 2019 MAFFT online service: multiple sequence alignment, interactive sequence choice and visualization. *Brief. Bioinform.*, 20:1160-1166.

Kazama, F. 1972. Ultrastructure of *Thraustochytrium* sp. zoospores, I. Kinetosomes. *Arch. Mikrobiol*., 83:179-188.

Kazama, F. 1980. The zoospore of *Schizochytrium aggregatum*. *Can. J. Bot.*. 58:2434-2446.

Kim, S., Jeon, C. B., Park, M. G., Kim, S., Jeon, C. B. & Park, M. G. 2017. Morphological observations and phylogenetic position of the parasitoid nanoflagellate *Pseudopirsonia* sp. (Cercozoa) infecting the marine diatom *Coscinodiscus wailesii* (Bacillariophyta). *Algae*, 32(3):181-187.

King, N.. Hittinger, C. T. & Carroll, S. B. 2003. Evolution of key cell signaling and adhesion protein families predates animal origins. *Science*, 301:361-363.

King, N., Westbrook, M. J., Young, S. L., Kuo, A., Abedin, M., Chapman, J., Fairclough, S., Hellsten, U., Isogai, Y., Letunic, I., Marr, M., Pincus, D., Putnam, N., Rokas, A., Wright, K. J., Zuzow, R., Dirks, W., Good, M., Goodstein, D., Lemons, D., Li, W., Lyons,

J. B., Morris, A., Nichols, S., Richter, D. J., Salamov, A., Sequencing, J. G. I., Bork, P., A. Lim, W. A., Manning, G., Miller, W. T., McGinnis, W., Shapiro, H., Tjian, R., Grigoriev, I. V. & Rokhsar, D. 2008. The genome of the choanoflagellate *Monosiga brevicollis* and the origin of metazoans. *Nature*, 451:783-788.

Kristiansen, J. & Škaloud, P. 2017. Chrysophyta. *In:* Archibald, J, M., Simpson, A. G. B. & Slamovits, C. H. (ed.), Handbook of the Protists. 2nd ed. Springer, Cham. 331-366.

Kühn, S. F. 1997. *Victoriniella multiformis*, gen. et spec. nov. (incerta sedis), a polymorphic parasitoid protist infecting the marine diatom Coscinodiscus wailesiiGran & Angst (North Sea, German Bight). *Arch. Protistenk.*, 148(1-2):115-123.

Kühn, S. F., Drebes, G. & Schnepf, E. 1996. Five new species of the nanoflagellate *Pirsonia* in the German Bight, North Sea, feeding on planktic diatoms. *Helgoländer Meeresunters.*, 50:205-222.

Kühn, S., Medlin, L. & Eller, G. 2004. Phylogenetic position of the parasitoid nanoflagellate *Pirsonia* inferred from nuclear-encoded small subunit ribosomal DNA and a description of *Pseudopirsonia* n. gen. and *Pseudopirsonia mucosa* (Drebes) comb. nov. *Protist*, 155(2):143-156.

Lafferty, K. D., Allesina, S., Arim, M., Briggs, C. J., De Leo, G., Dobson, A. P., Dunne, J. A., Johnson, P. T. J., Kuris, A. M., Marcogliese, D. J., Martinez, N. D., Memmott, J., Marquet, P. A., McLaughlin, J. P., Mordecai, E. A., Pascual, M., Poulin, R. & Thieltges, D. W. 2008 Parasites in food webs: the ultimate missing links. *Ecol. Lett.*, 11:533-546.

Lamża, Ł. 2023. Diversity of 'simple' multicellular eukaryotes: 45 independent cases and six types of multicellularity. *Biol. Rev.*, 98(6):2188-2209.

Leipe, D. D., Tong, S. M., Goggin, C. L., Slemenda, S. B., Pieniazek, N. J. & Sogin, M. L. 1996. 16S-like rDNA sequences from *Developayella elegans*, *Labyrinthuloides haliotidis*, and *Proteromonas lacertae* confirm that the stramenopiles are a primarily heterotrophic group. *Eur. J. Protistol.*, 32(4):449-458.

Leonard, G., Labarre, A., Milner, D. S., Monier, A., Soanes, D., Wideman, J. G., Maguire, F., Stevens, S., Sain, D., Grau-Bove, X., Sebe-Pedros, A., Stajich, J. E., Paszkiewicz, K., Brown, M. W., Hall, N., Wickstead, B. & Richards, T. A. 2018). Comparative genomic analysis of the 'pseudofungus' *Hyphochytrium catenoides*. Open Biol., 8(1), 170184. doi: 10.1098/rsob.170184.Logares, R., Audic, S., Santini, S., Pernice, M. C., De Vargas, C. & Massana, R. 2012. Diversity patterns and activity of uncultured marine heterotrophic flagellates unveiled with pyrosequencing. *The ISME J.*, 6(10):1823-1833.

Lunney, C. Z. & Bland, C. E. 1976. Ultrastructural observations of mature and encysting zoospores of *Pythium proliferum* de Bary. *Protoplasma*, 90:119-137.

Maistro, S., Broady, P., Andreoli, C. & Negrisolo, E. 2017. Xanthophyceae. *In:* Archibald, J, M., Simpson, A. G. B. & Slamovits, C. H. (ed.), Handbook of the Protists. 2nd ed. Springer, Cham. 407-434.

Manton, I. 1964. The possible significance of some details of flagellar bases in plants. *J. Roy. Micr. Soc.*, 82:279-285.

Martel, C. M. 2009. Nitrogen-deficient microalgae are rich in cell-surface mannose: potential implications for prey biorecognition by phagotrophic protozoa. Braz. J. Microbiol., 40:86-89.

Massana, R., Del Campo, J., Sieracki, M. E., Audic, S. & Logares, R. 2014. Exploring the uncultured microeukaryote majority in the oceans: reevaluation of ribogroups within stramenopiles. *The ISME J.*, 8(4):854-866.

Massana, R., Castresana, J., Balagué, V., Guillou, L., Romari, K., Groisillier, A., Klaus Valentin, K. & Pedros-Alio, C. 2004. Phylogenetic and ecological analysis of novel marine stramenopiles. *App. Env. Microbiol.*, 70(6):3528-3534.

Massana, R., Gobet, A., Audic, S., Bass, D., Bittner, L., Boutte, C., Chambouvet, A., Christen, R., Claverie, J.-M., Decelle, J., Dolan, J. R., Dunthorn, M., Edvardsen, B., Forn, I., Forster, D., Guillou, L., Jaillon, O., Kooistra, W. H. C. F., Logares, R., Mahé, F., Not, F., Ogata, H., Pawlowski, J., Pernice, M. C., Probert, I., Romac, S., Richards, T., Santini, S., Shalchian-Tabrizi, K., Siano, R., Simon, N., Stoeck, T., Vaulot, D., Zingone, A. & de Vargas, C. 2015. Marine protist diversity in European coastal waters and sediments as revealed by high-throughput sequencing. *Env. Microbiol*., 17(10):4035-4049.

Massana, R., Terrado, R., Forn, I., Lovejoy, C. & Pedrós-Alió, C. 2006. Distribution and abundance of uncultured heterotrophic flagellates in the world oceans. *Env. Microbiol*., 8(9):1515-1522.

Massana, R., Unrein, F., Rodríguez-Martínez, R., Forn, I., Lefort, T., Pinhassi, J. & Not, F. 2009. Grazing rates and functional diversity of uncultured heterotrophic flagellates. *The ISME J*., 3(5):588-596.

de Meeûs, T. & Renaud, F. 2002. Parasites within the new phylogeny of eukaryotes. *Trends Parasitol*. 18:247-251.

Moestrup, Ø. 2000. The flagellate cytoskeleton: introduction of a general terminology for microtubular flagellar roots in protists. In: Leadbeater, B. S. C. & Green, J. C. (ed.), Flagellates. Unity, diversity and evolution. The Taylor & Franscis, London. 69-94.

Moriya, M., Nakayama, T. & Inouye, I. 2000. Ultrastructure and 18S rDNA sequence analysis of *Wobblia lunata* gen. et sp. nov., a new heterotrophic flagellate (stramenopiles, incertae sedis). *Protist*, 151(1):41-55.

Moriya, M., Nakayama, T. & Inouye, I. 2002. A new class of the stramenopiles, Placididea classis nova: description of *Placidia cafeteriopsis* gen. et sp. nov. *Protist*, 153(2):143-156.

Niklas, K. J. & Newman, S. A. 2013. The origins of multicellular organisms. *Evol. Dev*., 15:41-52.

Nguyen, L. T., Schmidt, H. A., Von Haeseler, A. & Minh, B. Q. 2015. IQ-TREE: a fast and effective stochastic algorithm for estimating maximum-likelihood phylogenies. *Mol. Biol. Evol*., 32:268-274.

Noguchi, F., Tanifuji, G., Brown, M. W., Fujikura, K. & Takishita, K., 2016. Complex evolution of two types of cardiolipin synthase in the eukaryotic lineage stramenopiles. *Mol. Phylogenet. Evol*. 101:133-141.

O'Kelly, C. J. & Patterson, D. J. 1996. The flagellar apparatus of *Cafeteria roenbergensis* Fenchel & Patterson, 1988 (Bicosoecales = Bicosoecida). *Eur. J. Protistol*., 32(2):216-226.

Owen, H. A., Mattox, K. R. & Stewart, K.D. 1990. Fine structure of the flagellar apparatus of *Dinobryon cylindricum* (Chrysophyceae). *J. Phycol*. 26:131-141.

Patterson, D. J. 1985. The fine structure of *Opalina ranarum* (Family Opalinidae): opalinid phylogeny and classification. *Protistologica*, 21:413-428.

Patterson, D. J. 1989. Stramenopiles: chromophytes from a protistan perspective. *In:* Green, J. C, Leadbeater, B. S. C. & Diver, W. L. (ed.), The chromophyte algae: problems and perspectives. Clarendon Press, Oxford. 357-379.

Perkins, F. O. 1974. Phylogenetic considerations of the problematic thraustochyriaceous-labyrinthulid-*Dermocystidium* complex based on observations of fine structure. *Veroff. Inst. Meeresfomch. Bremerh.*, 5(1):45-63.

Preisig, H. R. 1989. The flagellar base ultrastructure and phylogeny of Chromophytes. *In:* Green, J. C., Leadbeater, B. S. C. & Diver, W. L. (ed.), The chromophyte algae: problems and perspectives. Clarendon Press, Oxford. 167-187.

Randolph, L. R. & Powell, M. J. 1992. Ultrastructure of zoospores of the oomycete *Apodachlya pyrifera*. *Mycologia*, 84(5):768-780.

Reid, B., Morris, B. M. & Gow, N. A. 1995. Calcium-dependent, genus-specific, autoaggregation of zoospores of phytopathogenic fungi. *Exp. Mycol.*, *19*(3):202-213.

Ronquist, F., Teslenko, M., Van Der Mark, P., Ayres, D. L., Darling, A., Höhna, S., Larget, B., Liu, L., Suchard, M. A. & Huelsenbeck, J. P. 2012. MrBayes 3.2: efficient Bayesian phylogenetic inference and model choice across a large model space. *Syst. Biol.*, 61(3):539-542.

Savory, A. I., Grenville-Briggs, L. J., Wawra, S., van West, P. & Davidson, F. A. 2014. Auto-aggregation in zoospores of *Phytophthora infestans*: the cooperative roles of bioconvection and chemotaxis. *J. Roy. Soc. Interface*. 11(94), 20140017. doi:10.1098/rsif.2014.0017.

Schnepf, E., Deichgräber, G. & Drebes, G. 1978. Development and ultrastructure of the marine, parasitic Oomycete, *Lagenisma coscinodisci* Drebes (Lagenidiales): Formation of the primary zoospores and their release. *Protoplasma*, 94:263-280.

Schnepf, E., Drebes, G. & Elbrächter, M. 1990. *Pirsonia guinardiae*, gen. et spec. nov.: a parasitic flagellate on the marine diatom *Guinardia flaccida* with an unusual mode of food uptake. *Helgoländer Meeresunters.*, 44:275-293.

Schnepf, E. & Kühn, S. F. 2000. Food uptake and fine structure of *Cryothecomonas longipes* sp. nov., a marine nanoflagellate incertae sedis feeding phagotrophically on large diatoms. *Helgol. Mar. Res.*, 54:18-32.

Schnepf, E. & Schweikert, M. 1997. *Pirsonia*, phagotrophic nanoflagellates incertae sedis, feeding on marine diatoms: attachment, fine structure and taxonomy. *Arch. Protistenk.*, 147(3-4):361-371.

Schweikert, M. 2015. Biology of parasitic heterotrophic nanoflagellates: parasitoids of diatoms. *In:* Ohtsuka, S., Suzaki, T., Horiguchi, T., Suzuki, & N. Not, F. (ed.), Marine Protists: Diversity and Dynamics. Springer, Tokyo. 519-530.

Schweikert, M. & Schnepf, E. 1997. Light and electron microscopical observations on *Pirsonia punctigerae* spec., nov., a nanoflagellate feeding on the marine centric diatom *Thalassiosira punctigera*. *Eur. J. Protistol.*, 33(2):168-177.

Sebé-Pedrós, A., Irimia, M., del Campo, J., Parra-Acero, H., Russ, C., Nusbaum, C., Blencowe, B. J. & Ruiz-Trillo, I. 2013. Regulated aggregative multicellularity in a close unicellular relative of metazoa. *eLife*. 2, e01287. doi:10.7554/eLife.01287.001.

Shiratori, T., Nakayama, T. & Ishida, K. I. 2015. A new deep-branching stramenopile, *Platysulcus tardus* gen. nov., sp. nov. *Protist*, 166(3):337-348.

Shiratori, T., Thakur, R., Ishida, K. I. 2017. *Pseudophyllomitus vesiculosus* (Larsen and Patterson 1990) Lee, 2002, a poorly studied phagotrophic biflagellate is the first characterized member of stramenopile environmental clade MAST-6. *Protist*, 168(4):439-451.

Simon, M., Jardillier, L., Deschamps, P., Moreira, D., Restoux, G., Bertolino, P. & López-García, P. 2015. Complex communities of small protists and unexpected occurrence of typical marine lineages in shallow freshwater systems. *Environ. Microbiol.*, 17(10):3610-3627.

Skovgaard, A. 2014. Dirty tricks in the plankton: diversity and role of marine parasitic protists. *Acta Protozool.*, 53(1):51-62.

Suttle, C. A., Chan, A. M., Taylor, W. D. & Harrison, P. J. 1986. Grazing of planktonic diatoms by microflagellates. *J. Plankton Res.*, 8(2):393-398.

Sing, V. O. & Bartnicki-Garcia, S. 1975. Adhesion of *Phytophthora palmivora* zoospores: electron microscopy of cell attachment and cyst wall fibril formation. *J. Cell Sci.*, 18(1):123-132.

Takahashi, Y., Yoshida, M., Inouye, I. &Watanabe, M. M. 2014. *Diplophrys mutabilis* sp. nov., a new member of Labyrinthulomycetes from freshwater habitats. *Protist*, 165:50-65.

Teal, T. H., Guillemette, T., Chapman, M. & Margulis, L. 1998. *Acronema sippewissettensis* gen. nov. sp. nov., microbial mat bicosoecid (Bicosoecales = Bicosoecida). *Eur. J. Protistol*., 34(4):402-414.

Thakur, R., Shiratori, T. & Ishida, K. I. 2019. Taxon-rich multigene phylogenetic analyses resolve the phylogenetic relationship among deep-branching stramenopiles. *Protist*, 170(5), 125682. doi:10.1016/j.protis.2019.125682.

Tikhonenkov, D. V., Janouškovec, J., Mylnikov, A. P., Mikhailov, K. V., Simdyanov, T. G., Aleoshin, V. V. & Keeling, P. J. 2014. Description of *Colponema vietnamica* sp. n. and *Acavomonas peruviana* n. gen. n. sp., two new alveolate phyla (Colponemidia nom. nov. and Acavomonidia nom. nov.) and their contributions to reconstructing the ancestral state of alveolates and eukaryotes. *PLoS One*, 9(4), e95467. doi:10.1371/journal.pone.0095467.

Tikhonenkov, D. V., Mikhailov, K. V., Gawryluk, R. M. R., Belyaev, A. O., Mathur, V., Karpov, S. A., Zagumyonnyi, D. G., Borodina, A. S., Prokina, K. I., Mylnikov, A. P., Aleoshin, V. V. & Keeling, P. J. 2022. Microbial predators form a new supergroup of eukaryotes. *Nature*, 612(7941):714-719.Tong, S. M. 1995. *Developayella elegans* nov. gen., nov. spec., a new type of heterotrophic flagellate from marine plankton. *Eur. J. Protistol*., 31(1):24-31.

Ucko, M., Elbrächter, M. & Schnepf, E. 1997. A *Crypthecodinium cohnii*-like dinoflagellate feeding myzocytotically on the unicellular red alga *Porphyridium* sp. *Eur. J. Protistol.*, 32(2):133-140.

Ucko, M., Shrestha, R. P., Mesika, P., Bar-Zvi, D. & Arad, S. M. 1999. Glycoprotein moiety in the cell wall of the red microalga porphyridium sp.(rhodophyta) as the biorecognition site for the *Crypthecodinium cohnii*-like dinoflagellate. *J. Phycol*., 35(6):1276-1281.

van West, P., Appiah, A. A. & Gow, N. A. 2003. Advances in research on oomycete root pathogens. *Physiol. Mol. Plant Pathol.*, 62(2):99-113.

Windsor, D. A. 1998. Controversies in parasitology. Most of the species on Earth are parasites. *Int. J. Parasitol*., 28:1939-1941.

Weston, E. J., Eglit, Y. & Simpson, A. G. 2023. *Kaonashia insperata* gen. et sp. nov., a eukaryotrophic flagellate, represents a novel major lineage of heterotrophic stramenopiles. *J. Euk. Microbiol.*, e13003. doi:10.1111/jeu.13003.

Yubuki, N., Čepička, I. & Leander, B. S. 2016. Evolution of the microtubular cytoskeleton (flagellar apparatus) in parasitic protists. *Mol. Biochem. Parasitol.* 209(1-2):26-34.

Yubuki, N. & Leander, B. S. 2013. Evolution of microtubule organizing centers across the tree of eukaryotes. *Plant J.*, 75(2):230-244.

Yubuki, N., Leander, B. S. & Silberman, J. D. 2010. Ultrastructure and molecular phylogenetic position of a novel phagotrophic stramenopile from low oxygen environments: *Rictus lutensis* gen. et sp. nov. (Bicosoecida, incertae sedis). *Protist*, 161(2):264-278.

Yoo, J. & Kim, S. 2020. Infection of marine diatom *Coscinodiscus wailesii* (Bacillariophyceae) by the parasitic nanoflagellate *Pirsonia diadema* (Stramenopiles) from Yongho Bay in Korea. *Korean J. Environ. Biol*., 38(4):567-577.

Weiler, B. A., Sà, E. L., Sieracki, M. E., Massana, R. & Del Campo, J. 2021. *Mediocremonas mediterraneus*, a new member within the Developea. J. Euk. Microbiol., 68(1), e12825. doi:10.1111/jeu.12825.

Yoon, H. S., Hackett, J. D., Pinto, G. & Bhattacharya, D. 2002. The single, ancient origin of chromist plastids. *Proc. Natl. Acad. Sci. U.S.A.,* 99:15507-15512.

Zohdi, E. & Abbaspour, M. 2019. Harmful algal blooms (red tide): a review of causes, impacts and approaches to monitoring and prediction. *Int. J. Env. Sci.Technol*., 16:1789-1806.

FIGURE LEGEND

FIGURE 1.
Phylogenetic tree generated from Bayesian analysis of 18S rRNA gene sequences. The tree contains 75 stramenopile sequences, including sequences of 7 new pirsoniales strains and 2 prey strains (ochrophytes), and 5 outgroup sequences. Bayesian posterior probabilities (BPP, GTR+I+GAMMA4) and Maximum Likelihood (ML, GTR+GAMMA+I model) bootstrap values are indicated at branches (only values >0.8/>50 are shown); black dots indicate values of BPP = 1.00 and ML bootstrap = 100%; dt – different topology. Sequences generated in this study are shown in bold.

FIGURE 2. Scanning electron microscopy of fixed cells of new pirsoniales strains: (A,B) *Bordeauxia parva* gen. et sp. nov. strain Colp-p1; (C-E) *Bullionia fluviatilis* gen. et sp. nov. strain Pirs-vl, showing a predatory cell swallowing a prey cell of the diatom *Cyclotella meneghiniana* (C,D) and a starved cell (E); (F-I) *Feodosia pseudopoda* strain NY0226 (F,G) and strain Colp-S9 (H,I). Abbreviations: **an** – acronema, **af** – anterior flagellum, **avg** – anterior ventral groove, **f** – flagellum, **pf** – posterior flagellum; **vg** – ventral groove. Scale bars: A-H – 5 µm, I – 1 µm.

FIGURE 3. Phase contrast (A,B,H-K,M,S,T,W,X) and differential interference contrast (C-G,L,N-R,U,V,Y-AB) light micrographs of new pirsoniales strains. (A-F) *Bordeauxia parva* gen. et sp. nov. strain Colp-p1: swimming cells (A,B), attached cells with emerged pseudopodia (C,D), and resting cells (E,F). (G-M) *Bullionia fluviatilis* gen. et sp. nov. strain Pirs-vl: swimming cells (G-K), cell with a well-developed food vacuole (H), cells swallowing cells of the prey diatom *Stephanocyclus meneghiniana* (I-K), resting cell (L), dividing cell (M). (N-T) *Koktebelia satura* gen. et sp. nov. strains Colp-Nor6 (N-Q, T) and Colp-Nor4 (R,S): swimming cell (N), resting cells (O-T), including a cell with emerged pseudopodia (Q), cell with a swallowed cell of the prey red alga *Erythrolobus coxiae* (S), and cluster of cells (T). (U-AB) *Noirmoutieria diatomophaga* gen. et sp. nov. strain Pirs-sm2: swimming cells (U,W,X), cell with a swallowed cell of the prey diatom *Attheya* sp. (W), resting cells of regular (V,Y), round (Z), and irregular (AA,AB) shape, including resting cells with detached flagella (V,AA,AB). Abbreviations: **af** – anterior flagellum, **an** – anterior notch, **bg** – bulge from which flagella emerge, **cv** – contractile vacuole, **dp** – diatom prey, **fv** – food vacuole, **ld** – lipid droplets, **pf** – posterior flagellum, **ps** – pseudopodia, **ra** – red algae prey, **vg** – ventral groove. Scale bars: A-C, U-AB – 5 µm, T – 15 µm.

FIGURE 4. Differential interference contrast (A,B,U-X) and phase contrast (C-T) light micrographs of *Feodosia pseudopoda* gen. et sp. nov. strains NY0226 (A,B), KT49-10a (C,D,U-X), and Colp-S9 (E-J,N-S): swimming cells (A,C-F); resting cell with noticeable ventral groove (B); cells with swallowed cells of the prey diatom *Attheya* sp. (E, F) and food vacuoles with remains of diatom prey (C, D); cells with swallowed cells of the prey diatom *Licmophora* sp. (G-J); undigested *Licmophora* sp. frustules after predator attack (K); defecated lumps of deformed compressed frustules of diatom *Attheya* sp. (L, M); cells feeding on the diatom *Coscinodiscus radiatus* (N-Q); cells feeding on the diatom cf. *Pinnularia* sp. (R, S); cf. *Pinnularia* sp. frustule after predator attack, chloroplasts are released out through the damaged frustule (T); cell aggregation of starved cells (U); large irregular multiflagellated cells (V-X). Abbreviations: **af** – anterior flagellum, **bg** – bulge from which flagella emerge, **ch** – chloroplast, **dp** – diatom prey cell, **fv** – food vacuole, **pf** – posterior flagellum, **ps** – pseudopodia, **vg** – ventral groove. Scale bars: A-T, V-X – 10 µm, U – 20 µm.

FIGURE 5. Transmission electron micrographs of *Bordeauxia parva* gen. et sp. nov. strain Colp-p1: (A) oblique section showing the general cell structure; (B) transverse section at the middle part of the cell showing the ventral groove; (C) flattened vesicle with flocculent material; (D,E) mitochondria with tubular cristae and central filament in each crista (E, insert); (F) posterior flagellum; (G) Golgi apparatus adjacent to the nucleus; (H) dilations of endoplasmic reticulum with tubular mastigonemes; (I) microbody; (J-L) serial sections

showing microtubules (indicated by arrows) conically radiating from kinetosomes and surrounding the nucleus. Abbreviations: **fv** – food vacuole; **ga** – Golgi apparatus**; k1** – posterior kinetosome; **k2** – anterior kinetosome; **ld** – lipid droplets; **mt** – mitochondrium; **n** – nucleus; **nu** – nucleolus; **pf** – posterior flagellum**; ve** – flattened vesicles; **vg** – ventral groove. Scale bars: A – 1 μm, B-L – 500 nm.

FIGURE 6. Transmission electron micrographs of the flagellar apparatus of *Bordeauxia parva* gen. et sp. nov. strain Colp-p1: (A) longitudinal section of the anterior kinetosome; (B) proximal part of the posterior kinetosome connected with the nucleus by two nuclear bands; (C) distal connecting band between the kinetosomes; (D) proximal part of the posterior kinetosome with associated roots; (E) distal part of the kinetosome with transitional fibers; (F-I) serial sections of the kinetosomes connected with each other by a striated proximal band; (J-N) serial sections of the kinetosomes and associated roots and fibers; (O) posterior part of the cell showing joined r1 and two-rowed r2; (P,Q) serial sections of k1 with associated r3; (R) lateral side of the cell with left anterior root r4. Abbreviations: **ac** – annular connection; **ax** – axosome; **cf** – core fibrous material; **cw** – cartwheel structure; **db** – distal connecting band; **dh** – central dense hub; **fb** – additional fibers; **ga** – Golgi apparatus; **k1** – posterior kinetosome; **k2** – anterior kinetosome; **n** – nucleus; **nb** – nuclear bands; **r1** – left posterior root; **r2** – right posterior root; **r3** – ribbed right anterior root; **r4** – left anterior root; **sb** – striated proximal band; **tf** – transitional fibers; **th** – transitional helix; **tp** – transverse plate; **ve** – flattened vesicle. Scale bars: 250 nm.

FIGURE 7. Diagram illustrating the proximal part of the flagellar apparatus of *Bordeauxia parva* gen. et sp. nov. viewed from the ventral face (A) and general cell view and orientation of flagellar roots from the ventral side (B) and the lateral side (C). The diagram does not illustrate the nuclear bands connecting the posterior kinetosomes with the nucleus. Abbreviations: **af** – anterior flagellum; **cf** – fibrous core material of r2, **db** – distal connecting band, **fb** – additional fiber connecting r1 and r2 together and with k1; **k1** – posterior kinetosome; **k2** – anterior kinetosome; **n** – nucleus; **pf** – posterior flagellum; **r1** – left posterior root; **r2** – right posterior root; **r3** – ribbed right anterior root; **r4** – left anterior root; **sb** – proximal striated connecting band; **arrows** indicate nuclear papillae.

FIGURE 8. Transmission electron micrographs of *Feodosia pseudopoda*. (A-H) strain NY0226: (A) whole cell; (B,C) peripheral part of the cell with vesicles, microbody and multivesicular body; (D,E) intracellular bacteria and dilations of endoplasmic reticulum with tubular mastigonemes (see insert); (F) transverse section of the proximal part of the posterior kinetosome with associated r2; (G,H) serial sections of the nucleus and proximal parts of the kinetosomes. (I-P) strain KT49-10a: (I) longitudinal section of the whole cell; (J) transverse section of the whole cell through a large food vacuole; (K) part of cell showing the nucleus, mitochondrium, and longitudinal section of the posterior kinetosome; (L) mitochondria with tubular cristae; (M) longitudinal section of both kinetosomes; (N-P) serial sections of the posterior kinetosome and associated roots and fibers.
Abbreviations: **ac** – annular connection; **av** – probable acorn-V filaments; **ax** – axosome; **b** – symbiotic intracellular bacteria; **cf** – core fibrous material; **ct** – central thickening of transverse plate; **cw** – cartwheel structure; **db** – distal connecting band; **df** – diatom frustule; **dh** – central dense hub; **er** – endoplasmic reticulum; **fb** – additional fibers; **k1** – posterior kinetosome; **k2** – anterior kinetosome; **ld** – lipid droplets; **mb** – microbody; **mt** – mitochondrium; **mvb** – multivesicular body; **n** – nucleus; **nb** – nuclear bands; **np** – nuclear papilla; **nu** – nucleolus; **pf** – posterior flagellum; **r1** – left posterior root; **r2** – right posterior root; **sb** – striated proximal band; **tf** – transitional fibers; **th** – transitional helix; **tp** – transverse plate; **ve** – vesicle; **vg** – ventral groove. Scale bars: A, I, J – 1 μm, B-H, K-P – 250 nm.

FIGURE 9. Transmission electron micrographs of *Bullionia fluviatilis* gen. et sp. nov. strain Pirs-vl: (A) longitudinal section of whole cell; (B) transverse section of whole cell at the level

of the proximal part of the posterior kinetosome; (C) mitochondria with tubular cristae; (D) part of cell with Golgi apparatus, longitudinal section of the posterior kinetosome connected to the anterior kinetosome by the distal connecting band; (E) longitudinal section of the posterior kinetosome showing detailed transitional zone; (F,G) serial sections through the proximal part of the posterior kinetosome with associated posterior roots, and probable acorn-V filaments (G) at the point of transition from triplets (F) to doublets (G); (H-J) serial sections of the posterior kinetosome and associated roots and fibers, and striated nuclear bands connecting the kinetosome with the nucleus. Abbreviations: **ac** – annular connection; **ax** – axosome; **cf** – core fibrous material; **ct** – central thickening of transverse plate; **db** – distal connecting band; **dh** – central dense hub; **fb** – additional fibers; **ga** – Golgi apparatus**; k1** – posterior kinetosome; **k2** – anterior kinetosome; **ld** – lipid droplets; **mt** – mitochondrium; **n** – nucleus; **nb** – nuclear bands; **nu** – nucleolus; **r1** – left posterior root; **r2** – right posterior root; **th** – transitional helix; **tp** – transverse plate. Scale bars: A, B – 1 μm, C-I – 250 nm.

FIGURE 10. (A) Maximum likelihood (ML) 16S rRNA phylogenetic tree showing the position of the bacterial endosymbiont of *Feodosia pseudopoda* strain NY0226 within Gammaproteobacteria. The tree contains 102 gammaproteobacterial sequences and 7 outgroup sequences of Alphaproteobacteria. The tree was constructed using the TPM3+R6 sequence evolution model. Branches with 100% ML bootstrap values are indicated by black dots, values lower than 50% are not shown. The branch lengths denoted by double slash (//) was shortened (2×) to improve visualization. For the full tree, see Figure S3. (B-D) Different views of a single *F. pseudopoda* cell under Hoechst fluorescent staining showing the presence of four host nuclei (indicated by white arrows) and numerous endosymbiont bacteria. Scale bars: 5 μm.

SUPPORTING INFORMATION

FIGURE S1. Bayesian phylogenetic tree of 18S rRNA gene sequences. The tree contains 86 stramenopile sequences, including sequences of 7 new pirsoniales strains, 2 new ochrophyte strains (prey), 11 environmental sequences, and 5 outgroup sequences. Bayesian posterior probabilities (BPP, GTR+I+GAMMA4) and Maximum Likelihood (ML, TN+F+I+G4 model) bootstrap values are indicated at branches (only values >0.8/>50 are shown); black dots indicate values of BPP = 1.00 and ML bootstrap = 100%; dt – different topology. Sequences generated in this study are shown in bold.

FIGURE S2. Bayesian phylogenetic tree of 18S rRNA gene sequences. The tree contains 97 stramenopile sequences, including sequences of 7 new pirsoniales strains and 2 new ochrophyte strains (prey), and 7 outgroup sequences. Bayesian posterior probabilities (BPP, GTR+I+GAMMA4) and Maximum Likelihood (ML, TN+F+I+G4 model) bootstrap values are indicated at branches (values >0.8/>50 are shown); black dots indicate values of BPP = 1.00 and ML bootstrap = 100%; dt – different topology. Sequences generated in this study are shown in bold.

FIGURE S3. Maximum likelihood (ML) 16S rRNA phylogenetic tree showing the position of the bacterial endosymbiont of *Feodosia pseudopoda* strain NY0226 within Gammaproteobacteria. The tree contains 102 gammaproteobacterial sequences, and 7 outgroup sequences of Alphaproteobacteria. The tree was constructed using the TPM3+R6 sequence evolution model. Branches with 100% ML bootstrap values are indicated by black dots, values lower than 50% are not shown.

TABLE S1. Comparison of the identity in the 18S rRNA sequences of new pirsoniales strains.

TABLE S2. Morphological characteristics of all known Pirsoniales species.

Video S1. *Bullionia fluviatilis* strain Pirs-vl swimming and attached (resting) cells that swallowed diatoms, PhC ×63, water immersion.

Video S2. *Koktebelia satura* strain Colp-Nor6 attached (resting) cell with pseudopodia, DIC ×63, oil immersion.

Video S3. *Koktebelia satura* strain Colp-Nor6 cluster of cells, PhC ×63, water immersion.
Video S4. A *Noirmoutieria diatomophaga* strain Pirs-sm2 attached (resting) cell sheds off its flagellum, DIC ×100, oil immersion.
Video S5. *Feodosia pseudopoda* strain Colp-S9 attached (resting) cells with slowly undulating flagella, DIC ×100, oil immersion.
Video S6. *Feodosia pseudopoda* strain Colp-S9 multiflagellated swimming cell, DIC ×63, water immersion.
Video S7. *Feodosia pseudopoda* strain Colp-S9 multiflagellated resting cell with large food vacuole, DIC ×63, water immersion.
Video S8. *Feodosia pseudopoda* strain KT49-10a cell aggregation, DIC ×63, water immersion.

Table 1. Information about the studied strains and samples from which they were isolated

Species	Strain	Sample collection/culture source	Coordinates	Date
***Bordeauxia parva* gen. et sp. nov.**	Colp-p1	France, Talmont-sur-Gironde, Gironde estuary, Atlantic ocean	45°32'03.5"N 0°54'24.0"W	01.07.2021
Paraphysomonas lucasi Scoble et Cavalier-Smith, 2014	str-V			
***Bullionia fluviatilis* gen. et sp. nov.**	Pirs-vl	France, Normandie, Valmont, river Valmont	49°44'50.7"N 0°30'26.3"E	1.08.2022
	Colp-RSA11	France, Ile-de-France, Bullion, river Saint Anne	48°36'43.7"N 1°58'40.6"E	14.03.2021
Cyclotella meneghiniana Kütz., 1844	Diat-RSA1			
***Feodosia pseudopoda* Tikhonenkov et al., 2022**	NY0226	France, Plage de Jean Blanc near Saint-Tropez, Mediterranean sea	43°08'57.9"N 6°24'44.6"E	20.09.2019
	Colp-S9	Italy, Sicily, near the salt lake reserve, Mediterranean sea	36°48'02.6"N 15°05'41.1"E	05.08.2021
	KT49-10a	Russia, Krasnodar krai, Sennoy village, Taman Bay of Azov sea	45°19'29.8"N 36°59'58.5"E	15.08.2021
***Noirmoutieria diatomophaga* gen. et sp. nov.**	Pirs-sm2	France, Noirmoutier-en-l'Île, Atlantic ocean	47°01'12.3"N 2°14'43.0"W	2.08.2022
***Koktebelia satura* Tikhonenkov et al., 2022**	Colp-Nor4	France, Yport, La Manche	49°44'23.8"N 0°18'33.7"E	27.07.2023
	Colp-Nor6	France, Vaucottes, La Manche	49°44'17.7"N 0°17'26.9"E	27.07.2023
Cf. *Developayella* sp.	str-opiA	Russia, Sochi, Black sea	43°35'00.7"N 39°42'49.8"E	21.10.2021
Attheya sp.	NY0228	France, Saint-Tropez, Plage de Jean Blanc, Mediterranean sea	43°08'57.9"N 6°24'44.6"E	20.09.2019
Odontella granulata (Roper) Ross, 1986	D1-val	Spain, Valencia, Mediterranean sea	39°28'28.3"N 0°19'21.9"W	2.08.2023
Lithodesmium undulatum Ehrenberg, 1839	D10-val			
Cylindrotheca closterium (Ehrenberg) Reimann et Lewin, 1964	D11-val			
Amphiprora alata (Ehrenberg) Kützing, 1844	D4-Nor2	France, Fecamp, La Manche	49°45'47.1"N 0°21'47.2"E	27.07.2023
Parlibellus sp.	D5-Nor2			
cf. *Pinnularia* sp.	D6-1-Nor2			
Gyrosigma sp.	D6-2-Nor2			
Navicula sp.	D8-Nor2			
Tabellaria sp.	D12-Nor2			
Amphora sp.	D13-Nor2			
Coscinodiscus sp.	D14-Nor2			
Licmophora sp.	D2-Nor9	France, Etretat, La Manche	49°42'29.5"N 0°12'06.2"E	27.07.2023
Ditylum brightwelii (West) Grunow, 1885	CCMP359	Benjamin BAILLEUL	-	-

Phaeodactylum tricornutum Bohlin, 1897	CCMP2561	Benjamin BAILLEUL	-	-
Skeletonema costatum (Greville) Cleve, 1873	RCC1617	Benjamin BAILLEUL	-	-
Minidiscus spinulatus (Takano) Park et Lee in Park et al., 2017;	RCC4659	Benjamin BAILLEUL	-	-
Leptocylindrus danicus Cleve, 1889	CCMP1856	Benjamin BAILLEUL	-	-
Thalassiosira pseudonana Hasle et Heimdal, 1970	CCMP1335	Benjamin Bailleul	-	-
Opephora guenter-grassii	DCG 044	Benjamin Bailleul	-	-
Chaetoceros muelleri Lemmermann, 1898	CCAP 1010-3	Benjamin Bailleul	-	-
Porphyridium purpureum (Bory) Drew et Ross, 1965	CCAP 1388/4	Fabian van Beveren	-	-
Erythrolobus coxiae Scott et al., 2006	CCAP 1393/6	Fabian van Beveren	-	-
Galdieria sp.	ACUF613	Fabian van Beveren	-	-
Timspurckia oligopyrenoides Yang et al., 2010	CCAP 1393/1	Fabian van Beveren	-	-
Rhodella violacea (Kornmann) Wehrmeyer, 1971	SAG 115.79	Fabian van Beveren	-	-
Rhodaphanes brevistipitata West et al., 2007	CCAP 1387/1	Fabian van Beveren	-	-
Procryptobia sorokini (Zhukov, 1975) Frolov et al., 2001	B-69	Denis Tikhonenkov	-	-
Coscinodiscus radiatus Ehrenberg, 1840	PLY1	Varsha Mathur	-	-

Table 2. Prey range of new Pirsoniales species. Data from feeding experiments: + well suitable prey, predators consumed prey actively and multiplied fast; +/- predators did not actively pursue prey and only partially consumed it, multiplied slowly and eventually culture died; - predators did not consume this prey; n/d – no data

Species name	*Feodosia pseudopoda*			*Bordeauxia parva*	*Noirmoutieria diatomophaga*	*Koktebelia satura*	
Strain name	NY0226	Colp-S9	KT49-10a	Colp-P1	Pirs-sm2	Colp-Nor4	Colp-Nor6
Heterotrophic flagellates							
Procryptobia sorokini	-	+	+	-	+	+	+
Cf. *Developayella* sp.	-	-	-	-	-	+	+
Paraphysomonas lucasi	-	-	-	+	-	+	+
Diatom algae							
Attheya sp.	+	+	+	-	+	+	+
Chaetoceros muelleri	+	+	+	-	+/-	+	+
Coscinodiscus radiatus	-	+	-	-	n/d	-	-
Gyrosigma sp.	-	+/-	-	-	n/d	-	-
Licmophora sp.	-	+	+	-	n/d	-	-
Navicula sp.	+	+	+	-	n/d	-	-
Opephora guenter-grassii	+/-	+/-	+/-	-	+/-	+	+
cf. *Pinnularia* sp.	-	+	-	-	n/d	-	-
Tabellaria sp.	+	+	+	-	n/d	+/-	+/-
Thalassiosira pseudonana	+/-	+/-	+/-	-	-	+	+
Amphiprora alata, *Amphora* sp., *Coscinodiscus* sp., *Cylindrotheca Closterium*, *Lithodesmium undulatum*, *Odontella granulata*, *Parlibellus* sp.	-	-	-	-	n/d	-	-
Leptocylindrus danicus	-	-	-	-	-	-	-
Ditylum brightwelii, *Minidiscus spinulatus*, *Phaeodactylum tricornutum*, *Skeletonema costatum*	-	-	-	-	-	n/d	n/d
Red algae							
Erythrolobus coxiae	-	+	+	-	n/d	+	+
Galdieria sp.	-	-	-	-	n/d	+/-	+/-
Porphyridium purpureum	+/-	+	+	-	n/d	+	+
Rhodaphanes brevistipitata	-	-	-	-	n/d	+	+
Rhodella violacea	+/-	-	-	-	n/d	+	+
Timspurckia oligopyrenoides	-	-	-	-	n/d	+	+

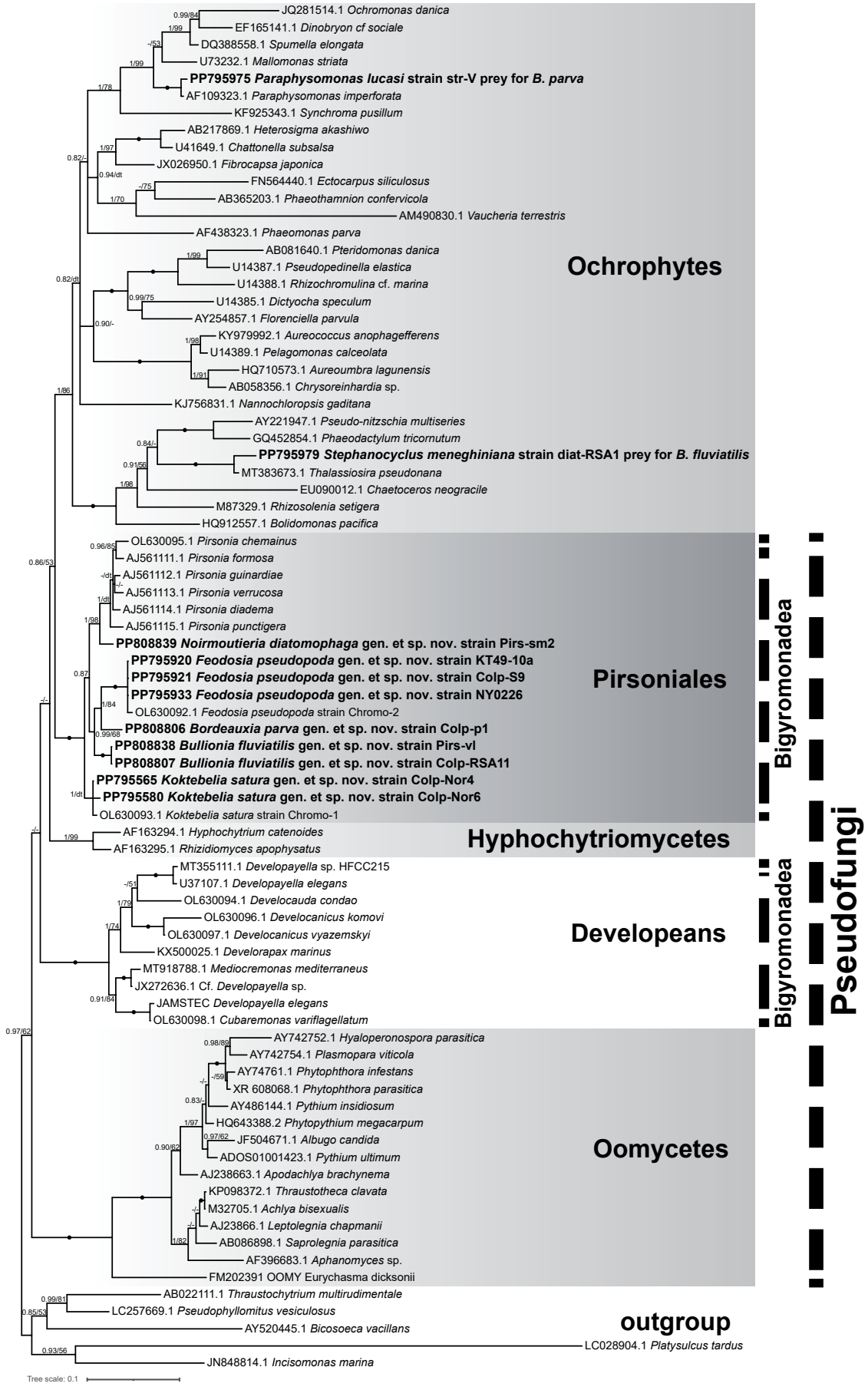
JQ281514.1 Ochromonas danica
EF165141.1 Dinobryon cf sociale
DQ388558.1 Spumella elongata
U73232.1 Mallomonas striata
PP795975 Paraphysomonas lucasi strain str-V prey for B. parva
AF109323.1 Paraphysomonas imperforata
KF925343.1 Synchroma pusillum
AB217869.1 Heterosigma akashiwo
U41649.1 Chattonella subsalsa
JX026950.1 Fibrocapsa japonica
FN564440.1 Ectocarpus siliculosus
AB365203.1 Phaeothamnion confervicola
AM490830.1 Vaucheria terrestris
AF438323.1 Phaeomonas parva
AB081640.1 Pteridomonas danica
U14387.1 Pseudopedinella elastica
U14388.1 Rhizochromulina cf. marina
U14385.1 Dictyocha speculum
AY254857.1 Florenciella parvula
KY979992.1 Aureococcus anophagefferens
U14389.1 Pelagomonas calceolata
HQ710573.1 Aureoumbra lagunensis
AB058356.1 Chrysoreinhardia sp.
KJ756831.1 Nannochloropsis gaditana
Ochrophytes
AY221947.1 Pseudo-nitzschia multiseries
GQ452854.1 Phaeodactylum tricornutum
PP795979 Stephanocyclus meneghiniana strain diat-RSA1 prey for B. fluviatilis
MT383673.1 Thalassiosira pseudonana
EU090012.1 Chaetoceros neogracile
M87329.1 Rhizosolenia setigera
HQ912557.1 Bolidomonas pacifica
OL630095.1 Pirsonia chemainus
AJ561111.1 Pirsonia formosa
AJ561112.1 Pirsonia guinardiae
AJ561113.1 Pirsonia verrucosa
AJ561114.1 Pirsonia diadema
AJ561115.1 Pirsonia punctigera
PP808839 Noirmoutieria diatomophaga gen. et sp. nov. strain Pirs-sm2
PP795920 Feodosia pseudopoda gen. et sp. nov. strain KT49-10a
PP795921 Feodosia pseudopoda gen. et sp. nov. strain Colp-S9
PP795933 Feodosia pseudopoda gen. et sp. nov. strain NY0226
OL630092.1 Feodosia pseudopoda strain Chromo-2
PP808806 Bordeauxia parva gen. et sp. nov. strain Colp-p1
PP808838 Bullionia fluviatilis gen. et sp. nov. strain Pirs-vl
PP808807 Bullionia fluviatilis gen. et sp. nov. strain Colp-RSA11
PP795565 Koktebelia satura gen. et sp. nov. strain Colp-Nor4
PP795580 Koktebelia satura gen. et sp. nov. strain Colp-Nor6
OL630093.1 Koktebelia satura strain Chromo-1
Pirsoniales
AF163294.1 Hyphochytrium catenoides
AF163295.1 Rhizidiomyces apophysatus
Hyphochytriomycetes
MT355111.1 Developayella sp. HFCC215
U37107.1 Developayella elegans
OL630094.1 Develocauda condao
OL630096.1 Develocanicus komovi
OL630097.1 Develocanicus vyazemskyi
KX500025.1 Develorapax marinus
MT918788.1 Mediocremonas mediterraneus
JX272636.1 Cf. Developayella sp.
JAMSTEC Developayella elegans
OL630098.1 Cubaremonas variflagellatum
Developeans
AY742752.1 Hyaloperonospora parasitica
AY742754.1 Plasmopara viticola
AY74761.1 Phytophthora infestans
XR 608068.1 Phytophthora parasitica
AY486144.1 Pythium insidiosum
HQ643388.2 Phytopythium megacarpum
JF504671.1 Albugo candida
ADOS01001423.1 Pythium ultimum
AJ238663.1 Apodachlya brachynema
KP098372.1 Thraustotheca clavata
M32705.1 Achlya bisexualis
AJ23866.1 Leptolegnia chapmanii
AB086898.1 Saprolegnia parasitica
AF396683.1 Aphanomyces sp.
FM202391 OOMY Eurychasma dicksonii
Oomycetes
AB022111.1 Thraustochytrium multirudimentale
LC257669.1 Pseudophyllomitus vesiculosus
AY520445.1 Bicosoeca vacillans
outgroup
LC028904.1 Platysulcus tardus
JN848814.1 Incisomonas marina
Tree scale: 0.1
Bigyromonadea
Bigyromonadea
Pseudofungi

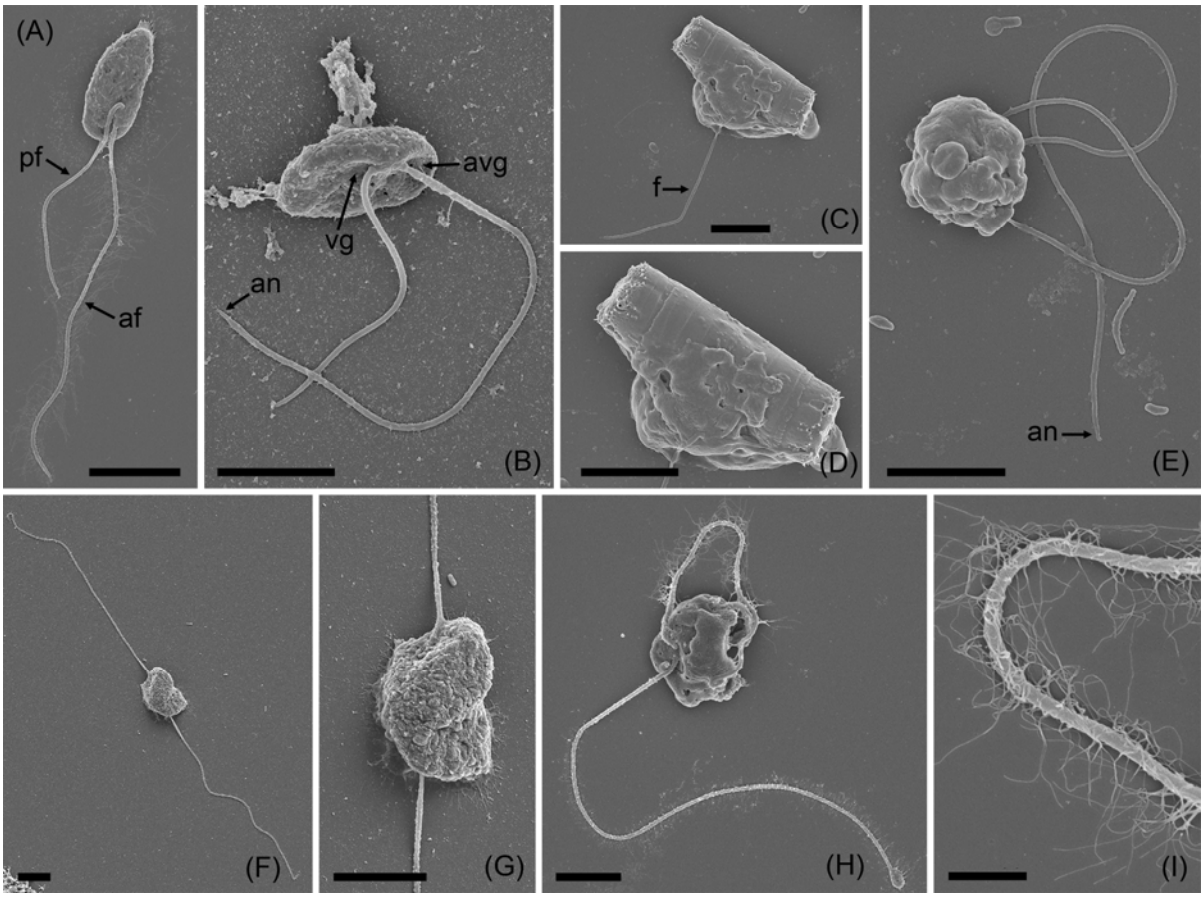

Figure 2

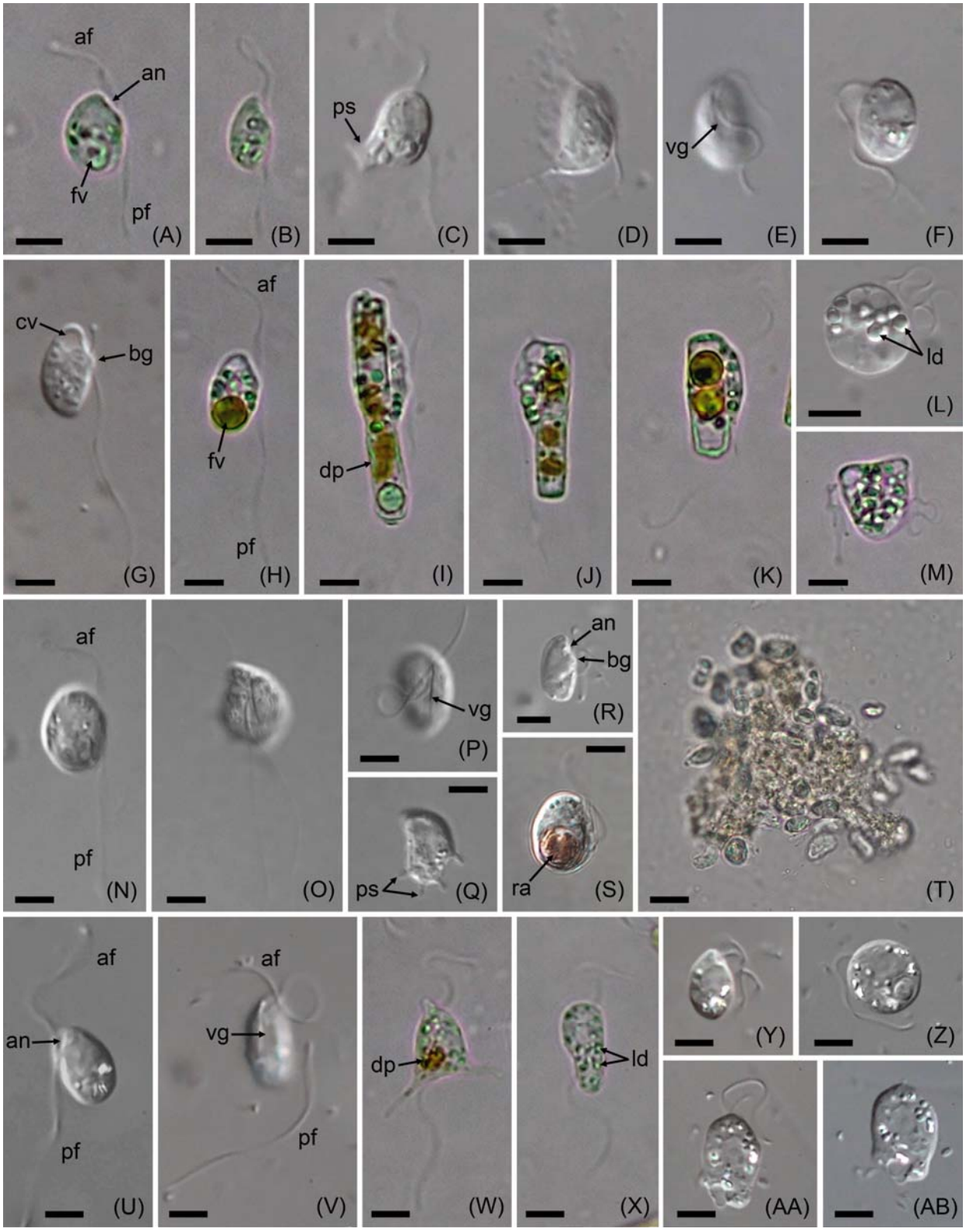
af
an
fv
pf
(A)
(B)
ps
(C)
(D)
vg
(E)
(F)
cv
bg
(G)
af
fv
pf
(H)
dp
(I)
(J)
(K)
ld
(L)
(M)
af
pf
(N)
(O)
vg
(P)
ps
(Q)
an
bg
(R)
ra
(S)
(T)
af
an
pf
(U)
af
vg
pf
(V)
dp
(W)
ld
(X)
(Y)
(Z)
(AA)
(AB)

Figure 3

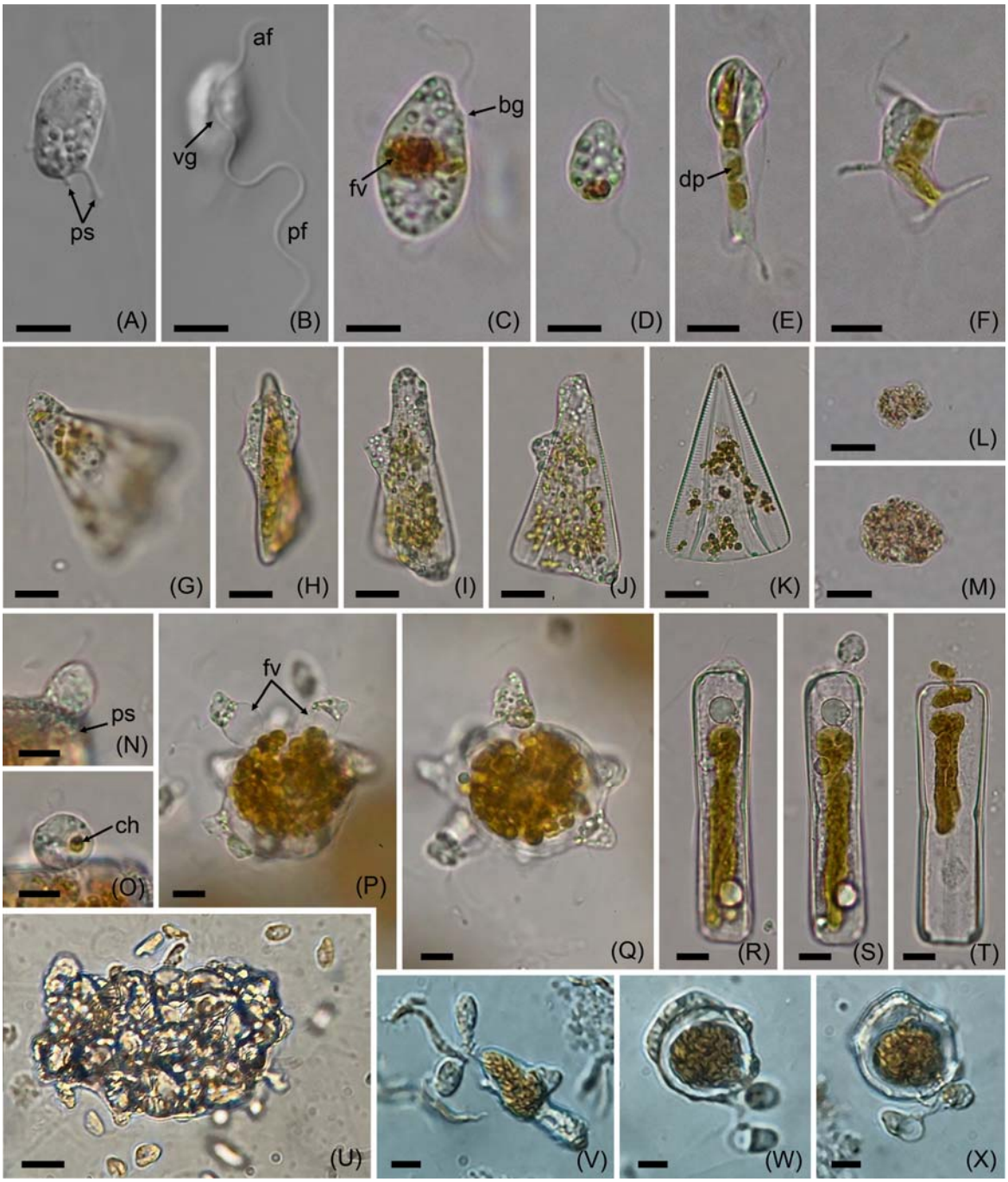

Figure 4

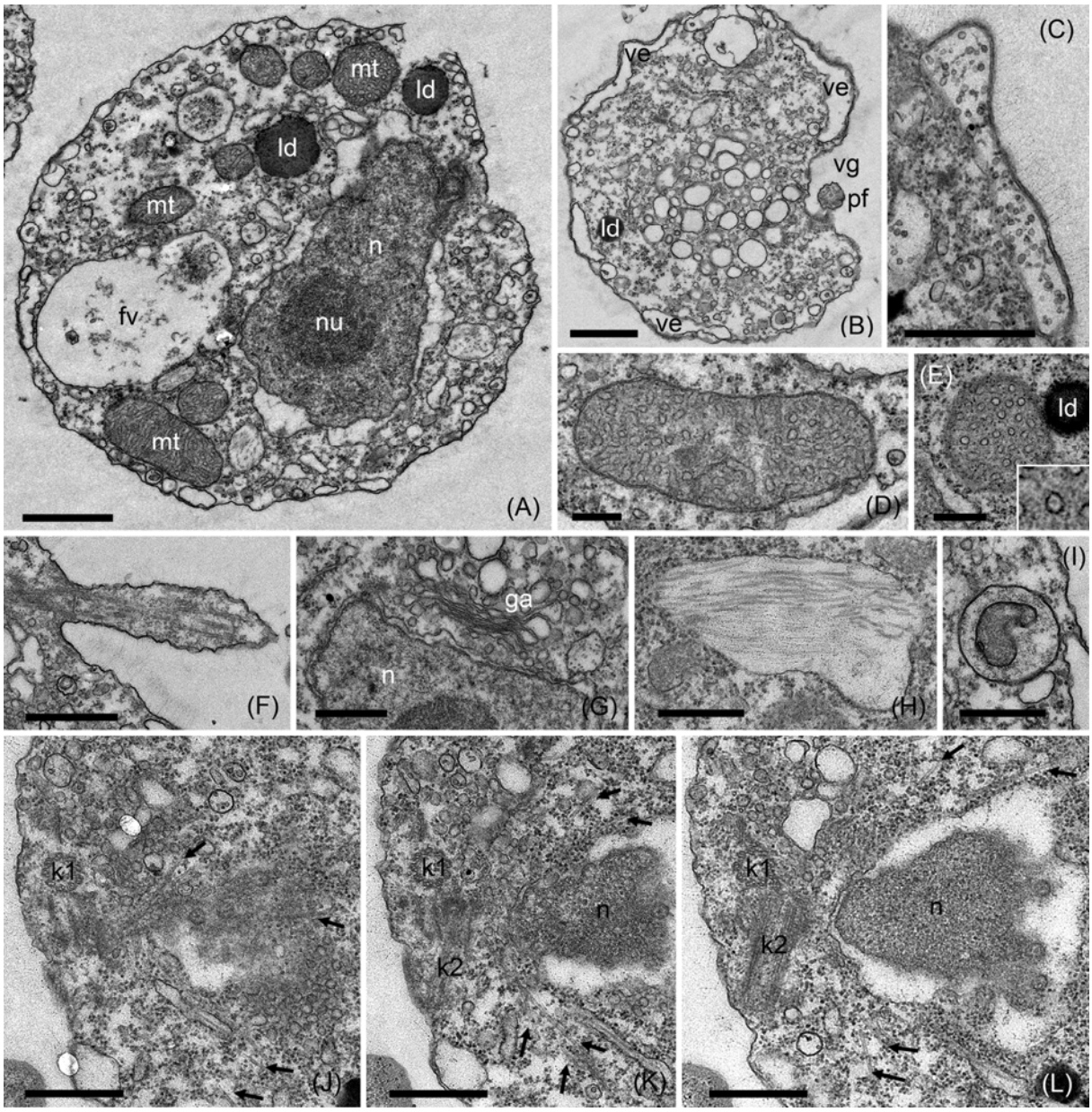
mt
ld
ld
mt
n
fv
nu
mt
(A)
ve
ve
vg
pf
ld
ve
(B)
(C)
(D)
(E)
ld
(F)
ga
n
(G)
(H)
(I)
k1
(J)
k1
n
k2
(K)
k1
n
k2
(L)

Figure 5

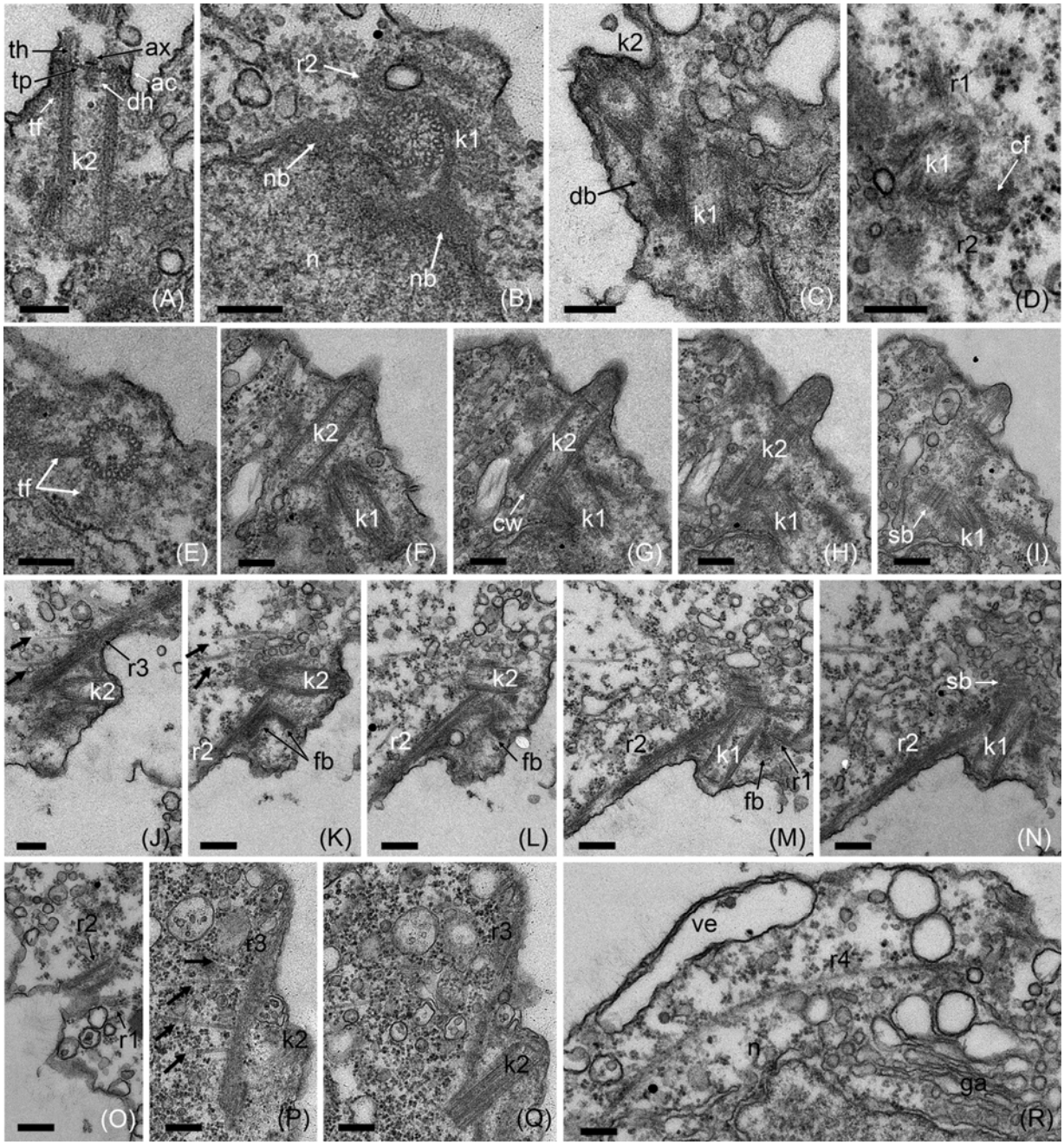
th
ax
tp
ac
dh
tf
k2
(A)
r2
k1
nb
n
nb
(B)
k2
db
k1
(C)
r1
cf
k1
r2
(D)
tf
(E)
k2
k1
(F)
k2
cw
k1
(G)
k2
k1
(H)
sb
k1
(I)
r3
k2
(J)
k2
r2
fb
(K)
k2
r2
fb
(L)
r2
k1
fb
r1
(M)
sb
r2
k1
(N)
r2
r1
(O)
r3
k2
(P)
r3
k2
(Q)
ve
r4
n
ga
(R)

Figure 6

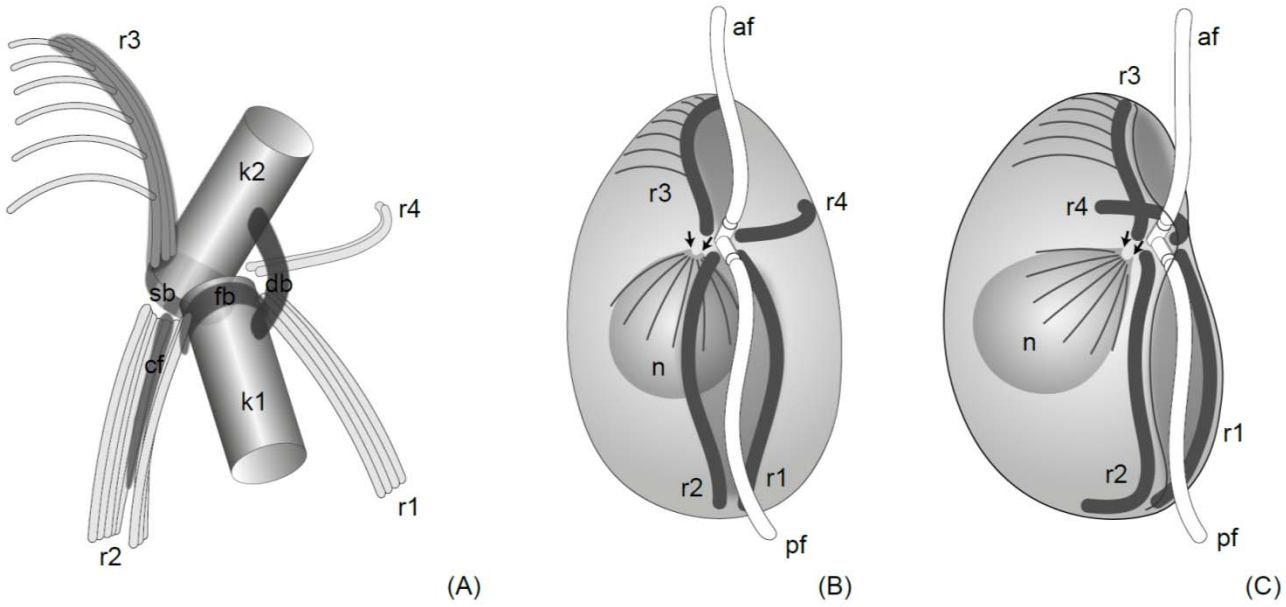

Figure 7

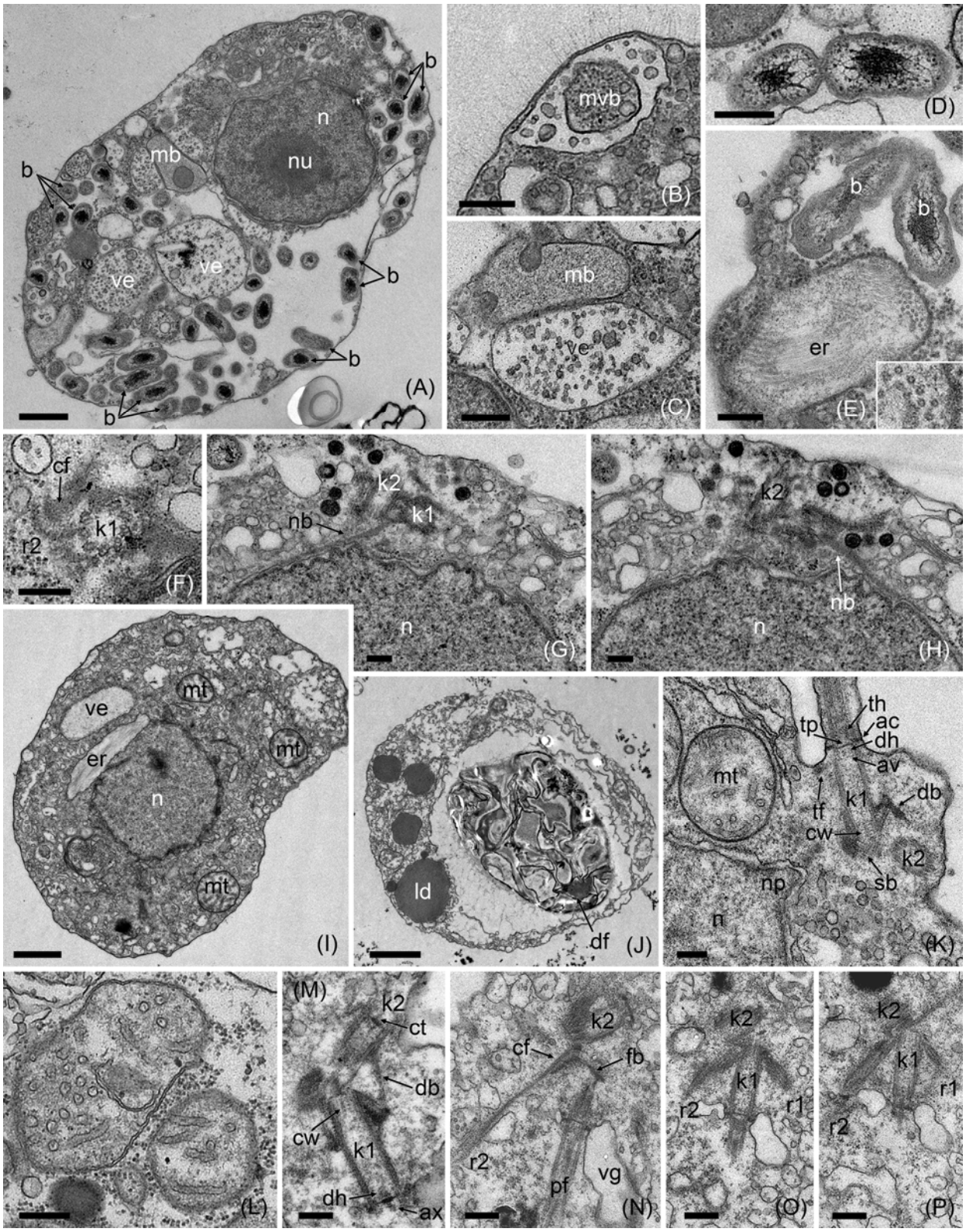
b
n
nu
mb
ve
(A)
mvb
(B)
(C)
(D)
er
(E)
cf
k1
r2
(F)
k2
nb
(G)
(H)
mt
(I)
ld
df
(J)
th
ac
dh
av
tp
tf
cw
db
sb
np
(K)
(L)
(M)
ct
ax
fb
pf
vg
(N)
r1
(O)
(P)

Figure 8

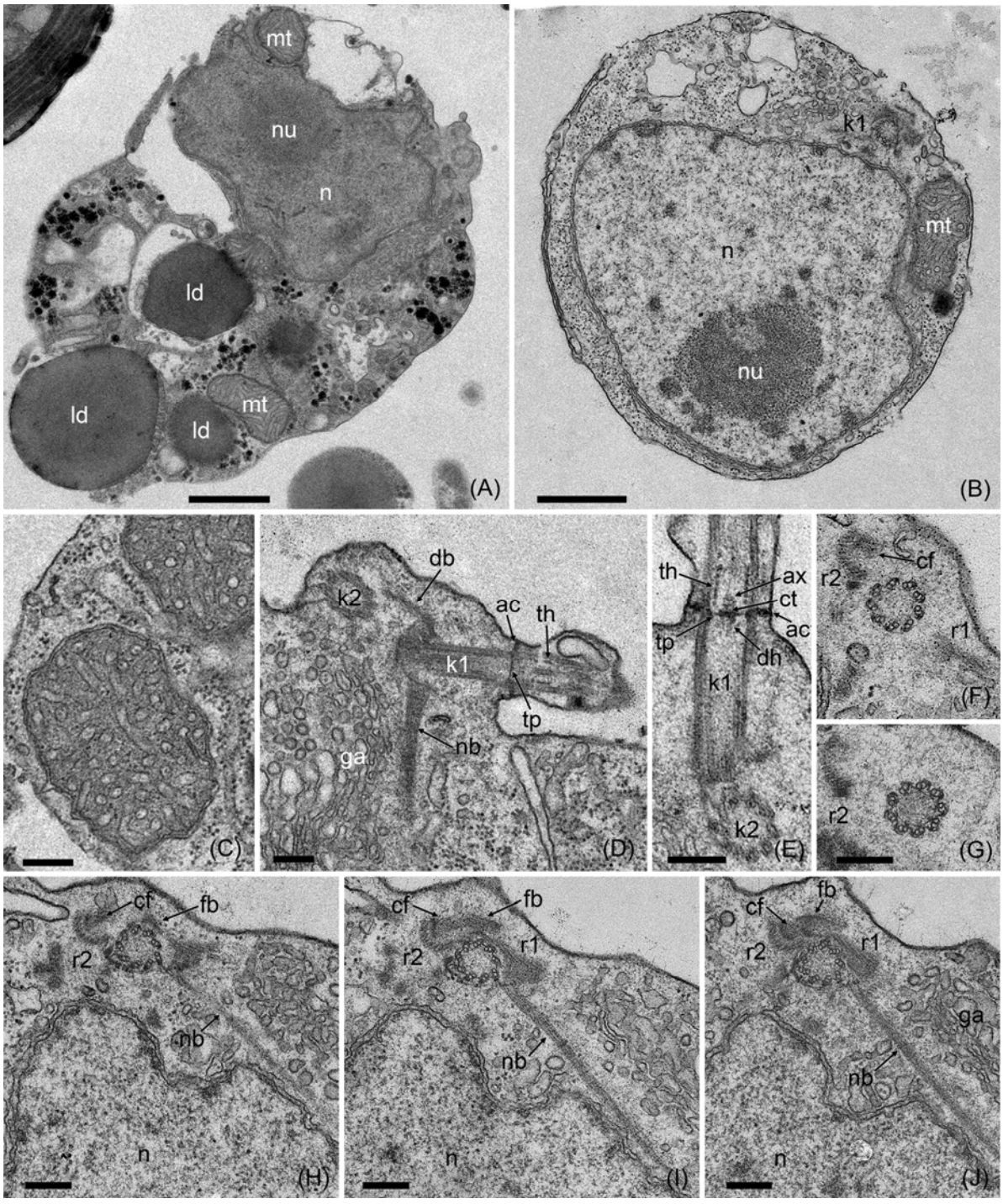
mt
nu
n
ld
ld
mt
ld
(A)
k1
mt
n
nu
(B)
(C)
db
k2
ac
th
k1
tp
ga
nb
(D)
th
ax
ct
ac
tp
dh
k1
k2
(E)
cf
r2
r1
(F)
r2
(G)
cf
fb
r2
nb
n
(H)
cf
fb
r1
r2
nb
n
(I)
cf
fb
r1
r2
ga
nb
n
(J)

Figure 9

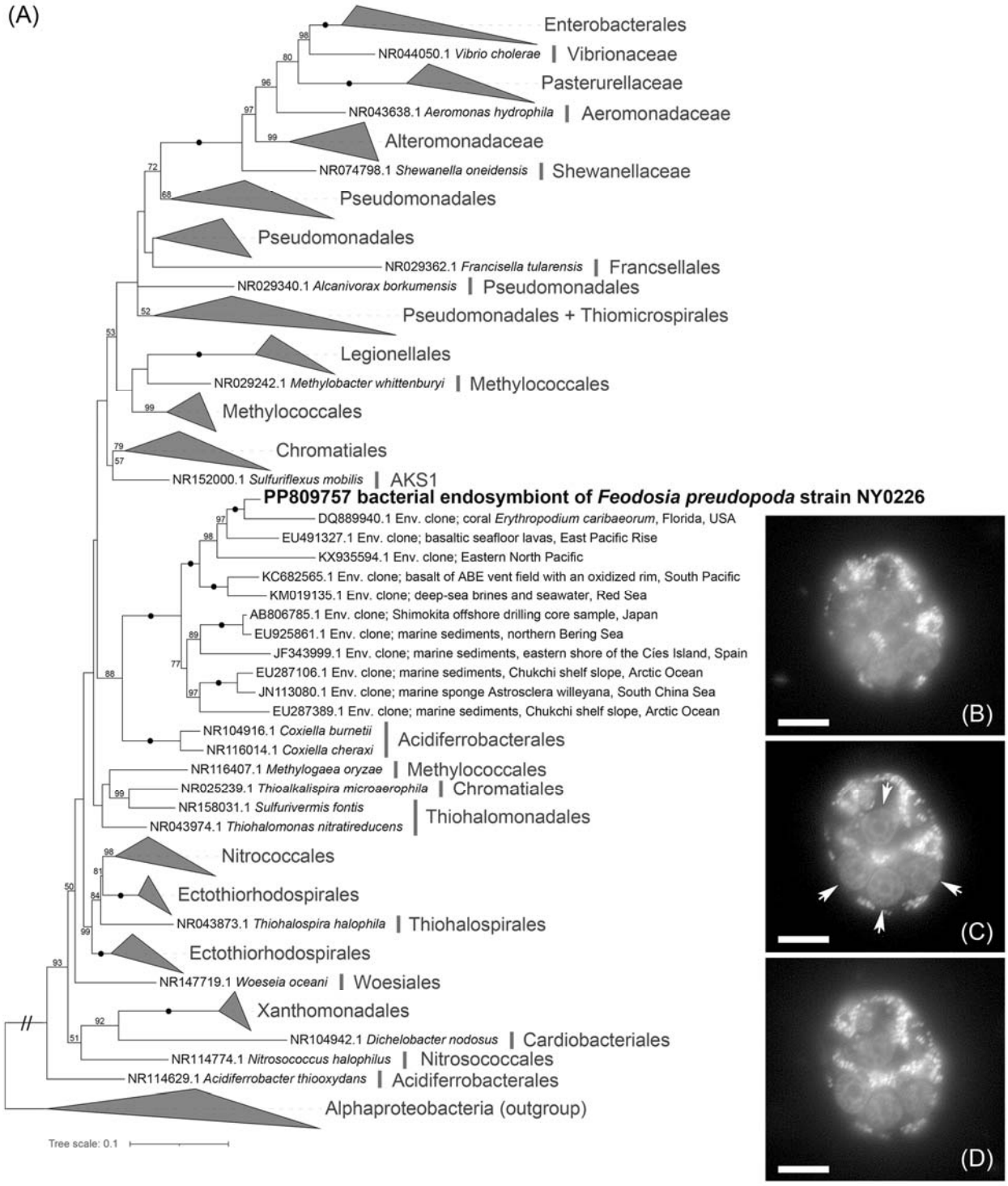
(A)
Enterobacterales
NR044050.1 Vibrio cholerae | Vibrionaceae
Pasterurellaceae
NR043638.1 Aeromonas hydrophila | Aeromonadaceae
Alteromonadaceae
NR074798.1 Shewanella oneidensis | Shewanellaceae
Pseudomonadales
Pseudomonadales
NR029362.1 Francisella tularensis | Francsellales
NR029340.1 Alcanivorax borkumensis | Pseudomonadales
Pseudomonadales + Thiomicrospirales
Legionellales
NR029242.1 Methylobacter whittenburyi | Methylococcales
Methylococcales
Chromatiales
NR152000.1 Sulfuriflexus mobilis | AKS1
PP809757 bacterial endosymbiont of Feodosia preudopoda strain NY0226
DQ889940.1 Env. clone; coral Erythropodium caribaeorum, Florida, USA
EU491327.1 Env. clone; basaltic seafloor lavas, East Pacific Rise
KX935594.1 Env. clone; Eastern North Pacific
KC682565.1 Env. clone; basalt of ABE vent field with an oxidized rim, South Pacific
KM019135.1 Env. clone; deep-sea brines and seawater, Red Sea
AB806785.1 Env. clone; Shimokita offshore drilling core sample, Japan
EU925861.1 Env. clone; marine sediments, northern Bering Sea
JF343999.1 Env. clone; marine sediments, eastern shore of the Cíes Island, Spain
EU287106.1 Env. clone; marine sediments, Chukchi shelf slope, Arctic Ocean
JN113080.1 Env. clone; marine sponge Astrosclera willeyana, South China Sea
EU287389.1 Env. clone; marine sediments, Chukchi shelf slope, Arctic Ocean
NR104916.1 Coxiella burnetii
NR116014.1 Coxiella cheraxi | Acidiferrobacterales
NR116407.1 Methylogaea oryzae | Methylococcales
NR025239.1 Thioalkalispira microaerophila | Chromatiales
NR158031.1 Sulfurivermis fontis
NR043974.1 Thiohalomonas nitratireducens | Thiohalomonadales
Nitrococcales
Ectothiorhodospirales
NR043873.1 Thiohalospira halophila | Thiohalospirales
Ectothiorhodospirales
NR147719.1 Woeseia oceani | Woesiales
Xanthomonadales
NR104942.1 Dichelobacter nodosus | Cardiobacteriales
NR114774.1 Nitrosococcus halophilus | Nitrosococcales
NR114629.1 Acidiferrobacter thiooxydans | Acidiferrobacterales
Alphaproteobacteria (outgroup)
Tree scale: 0.1
(B)
(C)
(D)

Figure 10